Enhanced Modulation Characteristics of Optical Injection-Locked Lasers: A Tutorial

Erwin K. Lau, *Member, IEEE*, Liang Jie Wong, and Ming C. Wu, *Fellow, IEEE*

(Invited Paper)

***Abstract*—In this paper a tutorial of optical injection locking of semiconductor lasers is given, with particular emphasis on the enhancement of system parameters. Furthermore, physical intuition of each parameter enhancement is explained and practical design rules and trends are also shown.**

***Index Terms*—Injection locking, modulation frequency response, semiconductor lasers.**

I. Introduction

THE DIRECTLY modulated semiconductor laser has appeared in many optical applications due to its availability and low cost. It has seen use from its origin as integrated modulator and source for telecommunication applications to economical transmitters for metro-level data communications. While there is much exciting research in developing high-speed direct-modulated lasers [1], [2], many fundamental limitations of other system parameters still exist. Optical injection locking (OIL) of semiconductor lasers has provided many improvements over these parameters, making direct-modulated lasers a much more attractive choice as transmitters. Table I lists many of these fundamental limits and how OIL has been shown to improve their characteristics [3]–[17]. While many of these enhancements are of great interest to communications, they can also be used for improving system performance of various applications, from microwave frequency generation [18], [19] to high linearity RF photonics sources [20] to all-optical signal processing [21]. However, the system dynamics of OIL lasers have traditionally been rich and complex, making it difficult for the nonexpert to determine correct laser design and locking conditions that will optimize their system.

In this paper, we attempt to explore the physical origin of many of the laser characteristics enhanced by OIL. In addition, we derive analytical formulas and design trends to provide a means for the optical engineer to optimize the OIL system for their particular application.

Fig. 1 shows a general schematic of a direct-modulated, direct-detection injection-locked laser system. The basic objective is to inject light from the master laser into the slave laser.

TABLE I
A List of Fundamental Limitations of Direct-Modulated Lasers and the Improvement from OIL

	Fundamental limits	Benefit from OIL
Laser	Mode partition noise (Fabry-Perot laser)	Single-mode with side-mode suppression [3]
	Relaxation oscillation frequency	Enhanced relaxation oscillation frequency [4-6]
	Non-linear electron-photon coupling	Reduced nonlinearities [7, 8]
	Amplified spontaneous emission noise	Reduced RIN [8-12]
	Wavelength chirp (non-zero α parameter)	Reduced chirp [13-15]
Link	Differential quantum efficiency < 1	Increased link gain [16]
	Double-sideband modulation	Near-single-sideband modulation [17]

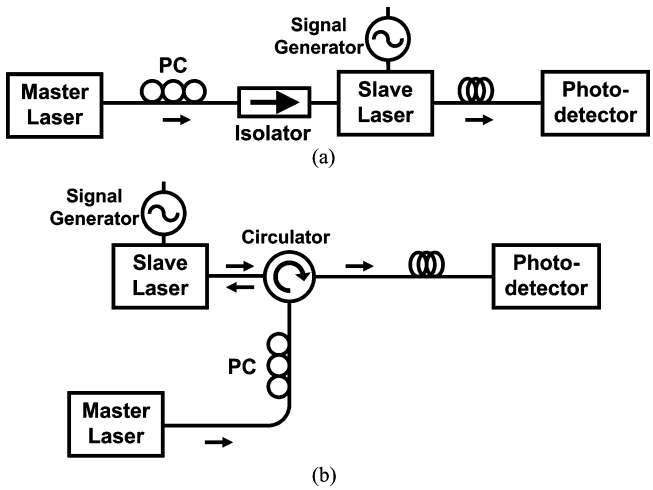

Fig. 1. Schematic of optical injection-locked laser system. (a) Transmission style. (b) Reflection style. PC: polarization controller.

An isolator is used to eliminate light coupling back to the master. There are two possible configurations of injection locking. In transmission-style injection locking [Fig. 1(a)], the injected master light enters one slave laser facet and the output is taken from the other facet. This necessitates two coupling systems on the slave laser. Oftentimes, for example, with vertical-cavity surface-emitting lasers (VCSELs), a reflection-style setup is used [Fig. 1(b)]. The output is taken at the same facet as the input of the injected light. An optical circulator is used to ensure that only the output beam goes to the photodetector. The reflection-style output is susceptible to reflected master light combining

Manuscript received November 15, 2008; revised December 19, 2008 and January 13, 2009. First published April 21, 2009; current version published June 5, 2009.

E. K. Lau and M. C. Wu are with the Department of Electrical Engineering and Computer Sciences, University of California, Berkeley, CA 94720-1774 USA (e-mail: elau@eecs.berkeley.edu; wu@eecs.berkeley.edu).

L. J. Wong is with the RF and Optical Department, Institute for Infocomm Research, Singapore 138632, Singapore (e-mail: liangjie@berkeley.edu).

Color versions of one or more of the figures in this paper are available online at http://ieeexplore.ieee.org.

Digital Object Identifier 10.1109/JSTQE.2009.2014779

with the slave laser facet output. This is important only in the strong injection regime and can be reduced by applying varying degrees of antireflection coating to the slave facet (while still maintaining a suitable threshold value). In either system, although polarization maintaining components are not necessary, a polarization controller is used to match the overlap of master and slave polarizations. Direct modulation is typically applied to the slave laser. A recently developed alternative is to use a ring laser as the slave [22], [23]. Injection via the master laser has been shown to suppress the reverse lasing direction, thus effectively suppressing back reflections and eliminating the need for an isolator, allowing the realization of integrated OIL systems.

Aside from typical parameters applied to a direct-modulated free-running laser, the OIL system has two primary parameters: the ratio of injected power from the master laser to the output power of the free-running slave, or injection ratio, and the difference between master and slave solitary lasing frequencies, or detuning frequency.

The process of injection locking is as follows. Light from the master is injected into the slave, not necessarily at the same wavelength. The master laser coherently combines with the slave light, causing a change in the slave laser's internal field, which deviates from its free-running value. Finally, when the dynamics of the laser settle, the slave wavelength is "pulled" toward the master wavelength until it equals that of the master, locking both its frequency and phase. Now, if the master laser frequency is changed, the slave will track this frequency until the frequency deviation from free running (detuning frequency $\Delta\omega_{\rm inj}$) becomes too large. At this point, the slave unlocks from the master and lases at its natural cavity wavelength. The span of frequencies that result in a locked state is the locking range. The locking range typically becomes larger as the ratio of master and slave optical powers defined as the injection ratio $R_{\rm inj}$ increases. Once locked, although the frequencies are the same, the relative phase between the slave and master (ϕ) can be nonzero, though its value depends on the detuning frequency and the injection ratio.

II. History

Perhaps the first recorded observation of injection locking was by Christiaan Huygens (1629–1695) [24], who noted that the pendulums on two clocks mounted on the same wall would eventually lock frequencies. A form of coupled oscillation, he reasoned that the pendulums would mechanically lock to one another by sending minute vibrations through the wall. The first published works of coupled oscillators emerged around 1920 in electrical systems. The earlier works characterized the synchronization of vacuum tube circuits as FM demodulators during the beginning of radio communications [25], [26]. It was during this era, in 1946, when Adler worked out the seminal differential equation that described the fundamental dynamics of electrical injection locking [27].

With the demonstration of the first laser oscillator in 1960 [28], injection locking was naturally translated to optical frequencies. The first OIL experiment, in 1966, used two HeNe lasers [29]. As new laser gain mediums were developed, injection locking of the medium usually followed a few years later, as in CO_2 lasers in 1972 [30] and, importantly for this work, semiconductor lasers in 1980 [31].

Much of the same theory and techniques of injection-locked electronic oscillators were applied to lasers. For example, several authors expanded Adler's equations to describe lasers [32]–[34], although it was in 1982 when Lang published the widely accepted standard OIL rate equations by taking in to account the linewidth enhancement parameter [35]. Additionally, with the advent of semiconductor lasers and low-loss optical fiber in the 1970s, coherent optical detection techniques were developed. As it did for electronics, injection locking provided a method for locking the local oscillator in coherent detection systems [36].

The 1980s saw rapid development of new phenomenon and applications for OIL systems. In 1982, Kobayashi and Kimura demonstrated optical phase modulation by direct modulation of the slave laser current [37]. The same authors developed FM with suppressed AM [38], which was later used by Kasapi *et al.* as a sub-shot-noise FM spectroscopy technique [39]. Pioneering work on hybrid optical/electrical injection-locked subsystems [40]–[42] also led to effective phase locking and modulation of phased array antennas [43]. Efficient optical microwave signal generation was developed by Goldberg, using sideband injection locking [19], [44]. Applications include distribution of microwave references, frequency multiplexing, and locking of microwave oscillators.

Coherent optical communications would eventually be eclipsed by the advent of the Erbium-doped fiber amplifier in the late 80s, making extremely long-haul direct-detection fiber links possible. In the field of direct detection, OIL has demonstrated several performance enhancements for both digital and analog optical communications. Reduction of chirp-induced dispersion of direct-modulated semiconductor lasers was first shown in 1984 [13]. Several groups [14], [15], [45] in the mid-80s demonstrated record bit rate-distance (B–L) products, pushing the limits of long-haul optical communications. Reduction of nonlinear distortions was demonstrated by Meng *et al*. [7] and Chrostowski *et al*. [8]. Reduction of relative intensity noise (RIN) and linewidth had been shown by several groups, both experimentally and theoretically [8]–[12], [46]–[48]. Additional enhancements are increased RF link gain [16] and near-single sideband modulation [17]. Finally, the enhancement of resonance frequency was proposed [4], [6] as a method for increasing modulation bandwidth for both analog and digital communications. The first RF spectra of resonance frequency enhancement was demonstrated in 1998 [49].

One of the main attractions of injection locking is that most or all of these enhancements are realized simultaneously. For example, simultaneous reduction in RIN and third-order intermodulation distortion with enhanced resonance frequency has been shown in our group, using injection-locked distributed Bragg reflector lasers [16], [50], and subsequently in VCSELs [20]. The resultant spurious-free dynamic range improvement was 5 dB and 20 dB, respectively. Although it was not measured at the time, chirp reduction could also be obtained at the same bias conditions. So, understanding the general mechanisms behind each effect allows us to optimize laser design as well as injection locking parameters to best suit the application on hand.

Although OIL has had a long history, the past decade has brought new and exciting advances. With the advent of economical, high-power semiconductor lasers, injection ratios of >0 dB can be realized. This strong OIL regime, for example, has allowed us to demonstrate greater than 100-GHz resonance frequencies and 80-GHz intrinsic 3-dB bandwidths [51]. Extrinsic bandwidths are, of course, limited by RC parasitics. However, by using the techniques discussed in Section IV-B, extrinsic 3-dB bandwidths of 44 GHz in distributed feedbacks (DFBs) [52] and 43.4 GHz in VCSELs [53] (49 GHz using double-polarization mode locking [54]) have been shown.

III. Basic Concepts

The foundations of all the analyses in this paper are the standard OIL rate equations [4], [5], [35], [55]:

$$\frac{dS(t)}{dt} = \{g[N(t) - N_{\rm tr}] - \gamma_P\} S(t) + 2\kappa\sqrt{S_{\rm inj}S(t)}\cos[\phi(t) - \phi_{\rm inj}] \quad (1)$$

$$\frac{d\phi(t)}{dt} = \frac{\alpha}{2}\{g[N(t) - N_{\rm tr}] - \gamma_P\} - \kappa\sqrt{\frac{S_{\rm inj}}{S(t)}}\sin[\phi(t) - \phi_{\rm inj}] - \Delta\omega_{\rm inj} \quad (2)$$

$$\frac{dN(t)}{dt} = J(t) - \gamma_N N(t) - g[N(t) - N_{\rm tr}]\, S(t) \quad (3)$$

where $S(t)$, $\phi(t)$, and $N(t)$ are the slave laser's photon number, field phase, and carrier number. $\phi(t)$ is the phase difference between slave and master: $\phi(t) \equiv \phi_{\rm slave}(t) - \phi_{\rm master}$. g, $N_{\rm tr}$, α, J, γ_N, and γ_P are the slave laser's linear gain coefficient, transparency carrier number, linewidth enhancement factor, current, carrier recombination rate, and photon decay rate, respectively. Gain compression, which primarily enhances the damping factor, is not modeled here. Since the damping factor can be modified by the locking conditions (see Section IV-B), gain compression becomes a secondary effect, so is neglected in this analysis for clarity. The injection terms κ, $S_{\rm inj}$, and $\Delta\omega_{\rm inj}$ are the coupling rate, injected photon number, and detuning frequency, respectively. The detuning frequency is formally defined as the difference between the master laser frequency $\omega_{\rm ML}$ and the free-running slave laser frequency $\omega_{\rm fr}$: $\Delta\omega_{\rm inj} \equiv \omega_{\rm ML} - \omega_{\rm fr}$. As injection ratio is more subtle, we describe it in Section III-C. In this work, we treat the injected photon number and phase as constants. In the general case, when they are allowed to change, this describes master amplitude and phase modulation and its application and analysis are discussed in [56].

The laser parameters used in this paper are listed in Table II, unless otherwise noted. Although length L and reflectivity r can be drastically different from laser to laser, we show in Section III-C that coupling-Q is a more important figure-of-merit. The linewidth enhancement factor α can vary greatly for different laser designs. For example, α has been measured as small as 0.1 or as large as 10 in quantum dot lasers [57], [58].

TABLE II
Injection-Locked Laser Parameters

Symbol	Value	Units
λ	1550	nm
g	4.7×10^4	1/s
N_{th}	2×10^7	#
α	5	-
J_{th}	2×10^{16}	1/s
J	$5\times J_{th}$	1/s
γ_N	1	1/ns
γ_P	500	1/ns
L	250	μm
r	0.25	-
κ	225	1/ns

A. Steady-State Solutions

Observing the trends of the steady-state solutions of (1)–(3) can give us insight into the enhanced dynamics to be studied. Here, we generally follow the solutions by Murakami *et al.* for the steady-state photon number, phase, and carrier number, defined here as S_0, ϕ_0, and N_0, respectively [5]. Solving for the free-running photon number $S_{\rm fr}$ in (3), we can set the above-threshold carrier number $\Delta N_0 \equiv N_0 - N_{\rm th}$ to zero, obtaining:

$$S_{\rm fr} = \frac{J - \gamma_N N_{\rm th}}{\gamma_P}, \quad (4)$$

where the threshold carrier number is $N_{\rm th} \equiv N_{\rm tr} + \gamma_P/g$. Using (4) and solving for the steady-state values of the injection-locked laser, we obtain:

$$S_0 = \frac{S_{\rm fr} - (\gamma_N/\gamma_P)\Delta N_0}{1 + (g\Delta N_0/\gamma_P)} \quad (5)$$

$$\phi_0 = \sin^{-1}\left\{-\frac{\Delta\omega_{\rm inj}}{\kappa\sqrt{1+\alpha^2}}\sqrt{\frac{S_0}{S_{\rm inj}}}\right\} - \tan^{-1}\alpha \quad (6)$$

$$\Delta N_0 = -\frac{2\kappa}{g}\sqrt{\frac{S_{\rm inj}}{S_0}}\cos\phi_0. \quad (7)$$

The mostconvenient solution is to choose an injection photon number $S_{\rm inj}$ and phase value ϕ_0 and knowing that the bounds of the phase across the locking range are approximately $\cot^{-1}\alpha$ to $-\pi/2$, from the negative to positive frequency detuning edges, respectively [48]. By choosing a ϕ_0 at which to solve the steady-state solutions, substituting (7) into (5), and defining a slave internal field strength A_0, normalized as $A_0^2 \equiv S_0$, yields a cubic equation

$$0 = S_0^{3/2} - \left[\frac{2\kappa}{\gamma_P}S_{\rm inj}^{1/2}\cos\phi_0\right]S_0 - S_{\rm fr}S_0^{1/2} - \frac{\gamma_N}{\gamma_P}\frac{2\kappa}{g}S_{\rm inj}^{1/2}\cos\phi_0 \quad (8)$$

whose roots $S_0^{1/2}$ can be easily solved by a numerical root-solving program. Then, (7) solves for ΔN_0, and we rearrange

TABLE III
STEADY-STATE LOCKING CONDITIONS AT SELECT VALUES IN THE LOCKING RANGE

	$\phi_0 = -\pi/2$	$\phi_0 = -\tan^{-1}\alpha$	$\phi_0 = 0$	$\phi_0 = \cot^{-1}\alpha$
$\Delta\omega_{inj}$	$+z$	0	$-\alpha z$	$-z\sqrt{1+\alpha^2}$
$\Delta\omega_{cav}$	0	$z\alpha/\sqrt{1+\alpha^2}$	$\Delta\omega_{inj}$	$-z\alpha^2/\sqrt{1+\alpha^2}$
$\Delta\omega_R$	$+z$	$z\alpha/\sqrt{1+\alpha^2}$	0	$z/\sqrt{1+\alpha^2}$
ΔN	0	$-2z/g\sqrt{1+\alpha^2}$	$-2z/g$	$-2z\alpha/g\sqrt{1+\alpha^2}$
S_0	S_{fr}	NS	NS	NS

NS: not shown, as there is no simple analytical expression available. $z = \kappa S_{inj}/S_0$.

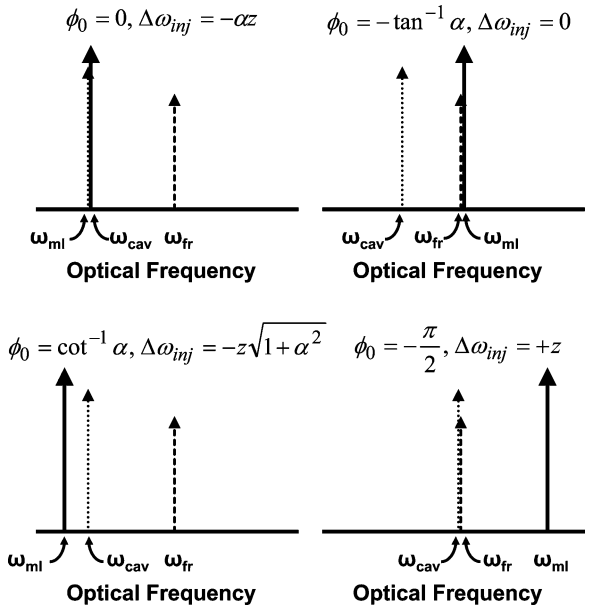

Fig. 2. Graphical representation of select detuning frequency values across the locking range. $\omega_{\rm ML}$: master laser frequency, $\omega_{\rm fr}$: free-running slave laser frequency, and $\omega_{\rm cav}$: cavity mode frequency.

(6) to determine the detuning frequency $\Delta\omega_{\rm inj}$:

$$\Delta\omega_{\rm inj} = -\kappa\sqrt{1+\alpha^2}\sqrt{\frac{S_{\rm inj}}{S_0}}\sin\left(\phi_0 + \tan^{-1}\alpha\right). \quad (9)$$

It is useful to gain some insight to the locking phenomenon by analyzing specific analytical cases in the locking range. The shift in the cavity mode from the free-running frequency $\Delta\omega_{\rm cav}$ is given by $\Delta\omega_{\rm cav} = \alpha g\Delta N/2$, and the resonance frequency enhancement $\Delta\omega_R$, as will be shown in Section IV-A, is the difference between master and cavity mode frequencies, given by $\Delta\omega_R = |\Delta\omega_{\rm inj} - \Delta\omega_{\rm cav}|$. Table III shows the position of the cavity mode and resonance frequency for specific detuning values. These are shown graphically in Fig. 2. Note that the maximum photon number for a given detuning frequency occurs for $\phi_0 = 0$, when the cavity mode overlaps with the locked frequency. In other words, the master is in resonance with the slave laser's cavity and adds fully in-phase with the slave light.

The steady-state values for the laser parameters in Table II are numerically simulated across the locking map in Fig. 3. Several qualitative trends can be noted. The photon number generally increases with an increase in injection power and/or negative detuning. The latter trend is primarily due to the nonzero α factor. This redshifts the cavity mode, necessitating a negative detuning to align the master and cavity mode frequencies. Should the α factor become 0, the cavity mode stays fixed at the free-running frequency, creating a symmetric locking map whose peak photon number will lie at a detuning frequency of 0 GHz. Additionally, Fig. 3(a) and (b) tells us that the photon number and carrier number will be close to the free-running value near the positive locking edge. Negative detuning will cause the carrier number to drop. Note that although the carrier number is below threshold, extra photon energy that was lost through output coupling or intrinsic loss is replenished by the injected master light. Hence, when locked, the slave laser continues to satisfy the gain = loss condition required for lasing.

B. Phasor Diagram

We can combine the photon and phase rate equations into a singular complex field rate equation:

$$\frac{dE(t)}{dt} = \frac{1}{2}g\Delta N E(t) + \kappa A_{\rm inj} - j\Delta\omega E(t) \quad (10)$$

where we have included the shift of the cavity mode with the frequency detuning term:

$$\Delta\omega \equiv \omega_{\rm ML} - \omega_{\rm cav} = -\frac{\alpha}{2}g\left(N_0 - N_{\rm th}\right) + \Delta\omega_{\rm inj}. \quad (11)$$

It is possible to explain the dynamics of injection locking via a phasor diagram. Henry *et al*. developed a phasor diagram model for injection-locked lasers that shows the effects of injected light on the slave field [4]. Another phasor diagram for electrical *LC* circuits can be found in [59]. In Fig. 4, we introduce a modified phasor diagram that shows the dynamics to achieve a steady-state injection-locked system. The phasor is in the frame-of-reference of the master laser frequency. Therefore, if the slave were lasing at the master laser frequency, the phasor would be static and would not rotate with time. To be locked, we desire the dynamic phasor vectors to sum to zero, resulting in a slave laser that is locked to the master. The angle of the phasor is the phase between master and slave, $\phi(t)$. However, the slave, even when locked, will lase at a frequency $\Delta\omega$ away from the master, and therefore will rotate $\Delta\omega\Delta t$ in a time interval, Δt, as shown in the last term in (10) and in vector 1 of Fig. 4. Since the injected master laser light has a phase equal to 0 in this frame-of-reference, the injected term is represented as a real vector, as shown in the second term on the right-hand side of (10) and in vector 2. Finally, the gain must reduce to lower the amplitude so that the slave field will return to steady state, shown in the first term of the right-hand side of (10) and vector 3.

This clearly shows that, despite being injection locked, the slave continues to emit photons at its cavity mode frequency. The injected master light serves to continually shift the phase of the slave so that it appears to lase at the frequency of the master. The phase-shifted cavity mode light then creates stimulated emission that is coherent to the new phase (but still at the cavity mode frequency), thereby sustaining the phase-shifting process. For example, this allows OIL DFB lasers to be locked in the middle

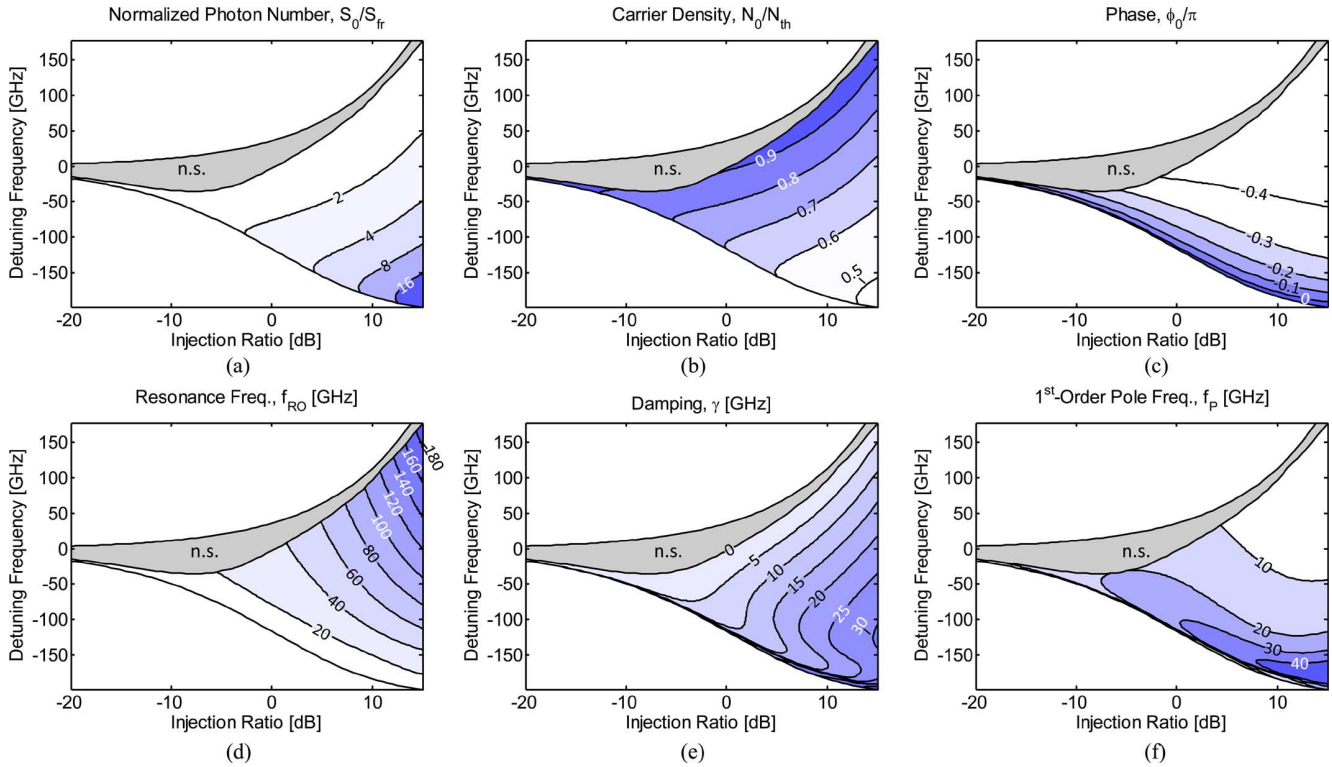

Fig. 3. Locking map for various injection locking states, showing steady state (a) photon number, (b) carrier number, and (c) phase. Dynamic values are also plotted, showing (d) resonance frequency, (e) damping factor, and (f) the first-order pole frequency. n.s.: unstable portion of the locking range.

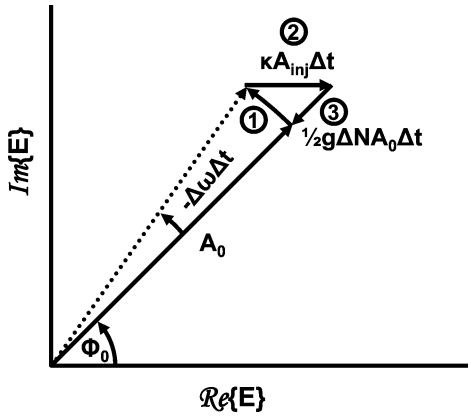

Fig. 4. Phasor model for injection locking, showing phasor perturbation in a time interval, Δt. Vector 1 corresponds to the free-running slave angular rotation, with respect to the frame-of-reference of the master laser frequency. Vector 2 is the vector addition of the injected master light at phase ϕ. Vector 3 is the reduction in amplitude due to the reduced gain.

of their stop band [51]. The injection-locked laser is very similar to a phase-locked loop, where a steady-state condition is only reached when the coherent addition of master and slave fields matches frequency with the master light. Finally, we see in Fig. 3(c) that the phase decreases, approaching $-\pi/2$, as the detuning is increased. Before it reaches this value, however, the OIL laser enters into an unstable locking condition, labeled "n.s.". This is further discussed in Section III-E.

C. Injection Ratio and Coupling Rate

Although the analysis calls for a specification for the injection photon number $S_{\rm inj}$, what actually is known is the injection *power*. The empirically measurable external power injection ratio is defined as the injected master power just before it is incident upon the slave's facet $P_{\rm inj}$ divided by the free-running slave power as it leaves the facet $P_{\rm fr}$ or

$$R_{\rm inj} \equiv \frac{P_{\rm inj}}{P_{\rm fr}}. \tag{12}$$

It is important to note that this definition only includes the field that couples to the slave's lasing mode; hence, coupling efficiency via polarization and mode matching are important. To relate the power ratio to the photon ratio just outside the facet, we can integrate the volume over the transverse mode area and a thin thickness projecting from the facet. Hence, the external power injection ratio is equivalent to the external photon ratio just outside the facet. To relate the external photon ratio outside the facet to the internal photon ratio in the cavity, the mirror reflectivity is used. The rate at which the injected photons enter into the cavity and distribute themselves along the cavity length L is defined as the coupling rate κ. An approximation for κ can be made by absorbing the internal/external injection ratio defined in [60] into its definition:

$$\kappa = \frac{v_g}{2L}\frac{1-r}{\sqrt{r}} = \frac{\omega_0}{2Q_c} \tag{13}$$

where Q_c is the coupling cavity quality factor (from mirror loss only) and r is the power reflectivity of the cavity mirrors. Hence, κ can be approximated as half the cold, lossless cavity bandwidth. Using this definition of κ allows us to define $S_{\rm inj}$ relative to the external free-running slave photon number and hence the power injection ratio. In other words, if an external power injection ratio of 3 dB is desired, we set $S_{\rm inj} = 2S_{\rm fr}$. Q_c is

typically in the 1000s, so $\kappa = 2\pi \times 36$ GHz (for $Q_c = 2700$). The coupling-Q, and therefore the coupling rate, is generally similar for different laser designs, from VCSELs to DFB lasers [60].

Note that this approximation holds for reflection-OIL lasers with linear cavities. Equation (13) would also hold for transmission-OIL lasers with equal facet reflectivities. Note also that the performance of the injection-locked system is more a function of the injection ratio, rather than the actual injection power. The external injection ratio can be defined as $R_{\text{inj}} \equiv S_{\text{inj}}/S_{\text{fr}}$, which is equivalent to (12). It is important to realize that this is not equivalent to the ratio S_{inj}/S_0, since the internal slave photon number rises above the free-running value as the laser is tuned to negative detuning frequencies.

D. Small-Signal Solutions

Although the injection locking rate equations are nonlinear coupled rate equations, much insight can be gleaned by analyzing them by a small-signal analysis. The linearized form of (1)–(3) can be placed in matrix form:

$$\begin{bmatrix} m_{SS}+j\omega & m_{S\phi} & m_{SN} \\ m_{\phi S} & m_{\phi\phi}+j\omega & m_{\phi N} \\ m_{NS} & 0 & m_{NN}+j\omega \end{bmatrix} \begin{bmatrix} \Delta S \\ \Delta\phi \\ \Delta N \end{bmatrix} = \begin{bmatrix} 0 \\ 0 \\ \Delta J \end{bmatrix} \tag{14}$$

where the matrix terms are

$$\begin{aligned} m_{SS} &= z\cos\phi_0 \\ m_{S\phi} &= 2zS_0\sin\phi_0 \\ m_{SN} &= -gS_0 \\ m_{\phi S} &= -z\sin\phi_0/2S_0 \\ m_{\phi\phi} &= z\cos\phi_0 \\ m_{\phi N} &= -\frac{1}{2}\alpha g \\ m_{NS} &= \gamma_P - 2z\cos\phi_0 \\ m_{NN} &= \gamma_N + gS_0 \end{aligned} \tag{15}$$

where $z \equiv \kappa\sqrt{S_{\text{inj}}/S_0}$ can be interpreted as the injection rate. Note that since S_0 changes over the locking range, as shown in Fig. 3(a), z also changes. For example, z decreases by up to a factor of 2 from the positive to the negative edge of the detuning range, for $R_{\text{inj}} = 5$ dB.

The magnitude of the direct modulation frequency response is then

$$\frac{\Delta S}{\Delta J} \equiv H(\omega) = M\frac{j\omega + Z}{(j\omega)^3 + A(j\omega)^2 + B(j\omega) + C} \tag{16}$$

where

$$\begin{aligned} A &= m_{SS} + m_{\phi\phi} + m_{NN} \\ B &= m_{SS}m_{\phi\phi} + m_{SS}m_{NN} + m_{\phi\phi}m_{NN} \\ &\quad - m_{S\phi}m_{\phi S} - m_{SN}m_{NS} \\ C &= m_{SS}m_{\phi\phi}m_{NN} + m_{S\phi}m_{\phi N}m_{NS} \\ &\quad - m_{S\phi}m_{\phi S}m_{NN} - m_{SN}m_{NS}m_{\phi\phi} \end{aligned}$$

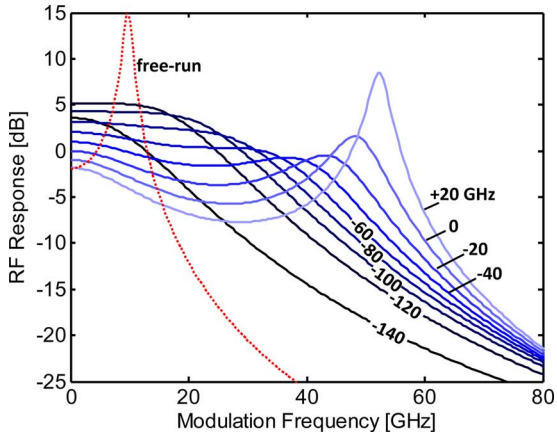

Fig. 5. Frequency response ($|H|^2$) curves for various detuning frequencies (labeled in GHz), at $R_{\text{inj}} = 4$ dB. The dotted curve is the free-running response.

$$\begin{aligned} Z &= \left(m_{S\phi}m_{\phi N} - m_{SN}m_{\phi\phi}\right)/m_{SN} \\ M &= -m_{SN}. \end{aligned} \tag{17}$$

Therefore, the frequency response can be easily determined by (16) and its auxiliary equations. The greater part of the direct modulation frequency response shape can be determined simply by analyzing the poles of the response function shown in (16). The zero frequency is typically much larger than any of the pole frequencies, so it can be treated as a constant. So, the frequency response can also be factored into its corresponding poles:

$$H(\omega) \approx \frac{ZM}{(j\omega + \omega_P)\left(j\omega - j\omega_R + \frac{1}{2}\gamma\right)\left(j\omega + j\omega_R + \frac{1}{2}\gamma\right)}. \tag{18}$$

Note that there will be two complex conjugate poles that will determine the resonance frequency ω_R and damping $-\gamma$, similar to a free-running laser. The resonance frequency and damping will be discussed in Sections IV-A and IV-B, respectively. In addition, there will be a first-order real pole $-\omega_P$ that will determine a low-pass filter response that factors greatly into the 3-dB bandwidth of the response. This will be discussed in-depth in Section IV-C. Before exploring analytical approximations to the OIL dynamics, a numerical look at these three dynamic parameters can give us a general optimization guideline of the frequency response. Fig. 3(d)–(f) plots the resonance frequency, damping, and first-order pole across the locking map. In general, the resonance frequency increases with injection ratio and detuning frequency. On the contrary, the damping factor increases with injection ratio but reduces with detuning frequency. Finally, the first-order pole increases with negative detuning. As an example, Fig. 5 plots the frequency response curves for various detuning frequencies, at a fixed injection ratio of $R_{\text{inj}} = 4$ dB. The trends just described are graphically shown in this figure.

E. Locking Range

The locking range is the range of detuning frequencies that satisfy conditions of stable locking and had been well studied in [48]. The first requirement for stable locking is determined by solving (6) for all valid values of ϕ_0, which must lie

between $\cot^{-1}\alpha$ to $-\pi/2$. The detuning frequencies that this corresponds to are

$$-z\sqrt{1+\alpha^2} < \Delta\omega_{\rm inj} < z. \tag{19}$$

Note that z is proportional to the cavity bandwidth via (13). As will be shown in Section IV-A, the locking range on the positive detuning side determines the maximum resonance frequency enhancement. Note also that the locking range boundaries in (19) are approximately proportional to the square root of the injection ratio: $\sqrt{S_{\rm inj}/S_0}$. As is shown in Fig. 3(a), $S_0 \approx S_{\rm fr}$ at the positive edge of the locking range. However, on the negative side, S_0 can be much larger that $S_{\rm fr}$ in the strong injection regime [see Fig. 3(a)], thus reducing frequency of the negative detuning edge. The second requirement for stable locking is that of stability; i.e., the poles must lie within the region of convergence (left-hand side of s-plane) and is usually solved numerically. This requires that the damping factor $-\gamma$ must be <0. This condition shrinks the locking range on the positive detuning side, when the resonance frequency damping goes to 0. This unstable region is labeled "n.s." in Fig. 3 and corresponds to the chaotic locking regime studied by several authors [61]–[63]. Although having significant impact at low to moderate injection ratios, this unstable region shrinks with stronger injection power and higher bias current to the degree that the chaotic regime no longer shows up in the experiment. Although the linewidth enhancement parameter increases the negative edge of the locking regime, it does not have an effect on the positive edge but does expand the unstable region to a greater fraction of the detuning range.

IV. Improved System Characteristics

In this section, we look at several system characteristics that can be enhanced by OIL. Here, we attempt to provide intuition to the physics behind each enhancement and delineate simple design guidelines that can be used to optimize the OIL system. The major system characteristics discussed here are resonance frequency enhancement, damping evolution, 3-dB small-signal bandwidth enhancement, chirp reduction, RIN reduction, and low-frequency RF gain.

A. Resonance Frequency Enhancement

One of the most powerful features of strong OIL is the ability to enhance the frequency of the slave laser's relaxation oscillation or resonance. Although this has been studied for almost a decade [4], [6], [64], only recently have we shown dramatic increases in the enhancement beyond 100 GHz by using strong injection powers [51].

We can approximate the resonance frequency as [55]

$$\omega_R^2 \approx -m_{SN}m_{NS} - m_{S\phi}m_{\phi S}. \tag{20}$$

The first term $m_{SN}m_{NS}$ is the resonance attributed to the dynamic coupling of the photons and carriers and approximates to the same physical origin of the relaxation oscillation of a free-running laser: $-m_{SN}m_{NS} \approx \omega_{R0}^2$, where $\omega_{R0}^2 = g\gamma_P S_{\rm fr}$. Using (15) to expand (20), the resonance frequency approximates to:

$$\omega_R^2 \approx \omega_{R0}^2 + \Delta\omega_R^2 \tag{21}$$

where the resonance frequency enhancement term $\Delta\omega_R$ is defined as the second term in (20):

$$\Delta\omega_R \equiv \sqrt{-m_{S\phi}m_{\phi S}} = \left|\kappa\sqrt{\frac{S_{\rm inj}}{S_0}}\sin\phi_0\right|. \tag{22}$$

From this, we found that the enhancement is proportional to the root of the injection power. Physically, the enhancement is attributed to the coupling of photons and phase. For example, if the master and slave initially start with a steady-state phase difference of $\phi_0 = 0$, the master and slave fields add coherently. If the phase is perturbed, the two fields add somewhat destructively and the effective photon amplitude decreases. This, in turn, causes the phase to readjust and the process repeats. Solving the steady-state condition of (2) and applying this to (22) yields

$$\Delta\omega_R = \left|-\frac{\alpha}{2}g\left(N_0 - N_{\rm th}\right) + \Delta\omega_{\rm inj}\right|. \tag{23}$$

As described by Murakami *et al*. [5], the resonance frequency enhancement is equal to the difference between the master laser frequency and that of the slave laser's natural cavity mode frequency. This cavity mode is redshifted by α via the first term in (23). Hence, for increasingly negative detuning frequencies, the master laser frequency approaches the cavity mode (see Fig. 2) and the resonance frequency enhancement decreases, as shown in Fig. 3(d). However, for positive detunings, the master moves in the opposite direction of the cavity mode migration, creating larger resonance frequency enhancements, with the larger enhancement occurring at the positive edge of the locking range. For low injection ratios, (21) reduces to the original free-running resonance frequency, which matches the experiment. When the enhancement is much larger than the free-running resonance frequency, the total resonance frequency approximates to the enhancement term, $\Delta\omega_R$. This enhancement can be over one order of magnitude greater than the free-running slave resonance frequency. As we see from (21), at very high enhancements, it is virtually irrelevant what the original free-running resonance is. Resonance enhancements from 3 GHz to >100 GHz have been demonstrated, limited only by the detection system [51]. The maximum enhancement is limited by the maximum stable frequency of the positive detuning edge. It scales with the square root of the injection ratio and is inversely proportional to the coupling-Q of the slave laser [60]:

$$\Delta\omega_{R,\max} \approx \frac{\omega_0}{2Q_c}\sqrt{R_{\rm inj}}. \tag{24}$$

Of course, another practical limitation to the enhancement is the slave laser's Fabry–Perot mode spacing. If the master laser detunes far enough away from the primary mode such that it approaches the frequency of an adjacent slave mode, it will lock to the adjacent mode. Hence, a larger mode spacing laser is desired for maximum resonance frequency enhancement. For a Fabry–Perot laser, this may only be 100 GHz, whereas a DFB could be >200 GHz and a VCSEL even larger.

B. Damping Factor

As in free-running lasers, the damping factor affects the peak amplitude of the resonance (see Fig. 5). As shown in Fig. 3(e), the damping factor also evolves with the locking parameters. It is important to understand these trends for optimization of the OIL laser to different applications. For example, a highly damped resonance is useful to eliminate relaxation oscillation ringing for digital modulation. On the other hand, a large peak value would be useful for narrow-band, high-gain applications, such as optoelectronic oscillators [65], [66].

The approximate damping factor for large damping values is [55]

$$\gamma \approx \gamma_0 - g\left(N_0 - N_{\rm th}\right) \tag{25}$$

where $\gamma_0 = \gamma_N + gS_0$ is the free-running damping term. The injection-locked laser's damping is the free-running damping enhanced by the reduction of gain below threshold. As the master laser field coherently adds photons to the slave cavity, the gain is reduced in order to maintain a steady state. This reduction in gain below threshold increases the damping of the resonance.

For small damping values, which occur near the positive edge of the detuning range [see Fig. 3(e)], the approximations used to derive (25) no longer hold and a modified damping term must be used:

$$\gamma_M\left(\phi \approx -\frac{\pi}{2}\right) \approx -g\Delta N - \frac{\kappa g S_0}{\omega_R^2}\sqrt{R_{\rm inj}}\left(\alpha\gamma_P + \kappa\sqrt{R_{\rm inj}}\right). \tag{26}$$

Hence, the carrier number must be sufficiently below threshold for the damping term to be positive and the solution to remain in the region of convergence. This causes the stable locking range to shrink, accounting for the boundary between stable locking and the chaotic locking regimes.

As an example, Fig. 6 shows experimental verification of the resonance frequency enhancement and damping factor reduction across the locking range [51]. In this experiment, the resonance frequency enhancement was limited only by the maximum network analyzer frequency of 110 GHz. The sharpening of the resonance shows the reduction of the damping frequency as the detuning approaches the positive locking range edge.

C. Bandwidth Enhancement

In a free-running laser, the damping fundamentally increases as the square of the resonance frequency [67]. This limits the laser bandwidth to g/ε, where ε is the gain compression factor. In OIL, the resonance frequency and damping are no longer bound by the free-running laser's fundamental relationship between resonance frequency and damping. In fact, as the detuning frequency is increased, the damping decreases as the resonance frequency is enhanced and the opposite trend found in a solitary laser. This allows for much larger freedom of design of the frequency response. If the OIL response was governed solely by this damped resonance, enhanced bandwidths would have been observed in the original demonstrations of OIL resonance frequency enhancement [64]. Rather, the OIL bandwidth is dominated by another dynamic: the first-order pole frequency ω_P, shown in (18). As shown in Fig. 3(d), (f), when the resonance frequency is enhanced, the pole frequency is much less than the resonance. This causes a 3-dB roll-off at a frequency much less than the resonance, effectively limiting the 3-dB bandwidth to $\sim\omega_P$. For $\Delta\omega_R > \omega_{R_0}$ (which is true when bandwidth enhancement over the free running is desired), an approximate value for ω_P can be derived:

$$\omega_P \approx \left[1 + \frac{\alpha}{\omega_R}\left(\gamma_P + g\Delta N\right)\right] gS_0. \tag{27}$$

The most important feature of the pole frequency is that it is proportional to gS_0. This means, first, that a large differential gain is attractive for large bandwidths. Most importantly, however, this means that the pole frequency is proportional to the photon number. Aside from using negative detuning frequencies, the pole frequency has been found to be enhanced by increasing the slave laser current bias [51], [55]. This realization has allowed bandwidth enhancements of the OIL laser to unprecedented levels: an intrinsic bandwidth of 80 GHz has been demonstrated [51]. Fig. 7 shows the intrinsic 3-dB bandwidths across the locking range for three bias levels: $J = 3\times$, $5\times$, and $10 \times J_{\rm th}$. The free-running 3-dB frequencies are 10.5, 15, and 22.5 GHz, respectively. The maximum 3-dB bandwidths within the locking range shown are 34, 49, and 76.5 GHz, respectively, which would signify a bandwidth enhancement of $\sim$3.3 times the free-running value. The region of largest bandwidth in Fig. 7(b), for example, corresponds to a first-order pole frequency of only $\sim$15 GHz, shown in Fig. 3(f). The bandwidth of $>$40 GHz is due to the $\sim$40-GHz resonance frequency pulling up the high-frequency response before the pole drops below 3-dB (see $\Delta\omega_{\rm inj} = -40$ GHz case in Fig. 5). Hence, the pole frequency need not be extremely high to result in greatly enhanced bandwidths. The significance of the abrupt drop in the 3-dB bandwidth in all three charts (e.g., from 70 to 20 GHz around $R_{\rm inj} = 5$ to 10 dB in (c)) is caused by the increase in the resonance frequency and drop in the pole frequency such that the resonance frequency is not able to pull the response up before the pole frequency causes a 3-dB drop in the response, thus once again dominating the 3-dB response (see $\Delta\omega_{\rm inj} \geq -20$ GHz cases in Fig. 5).

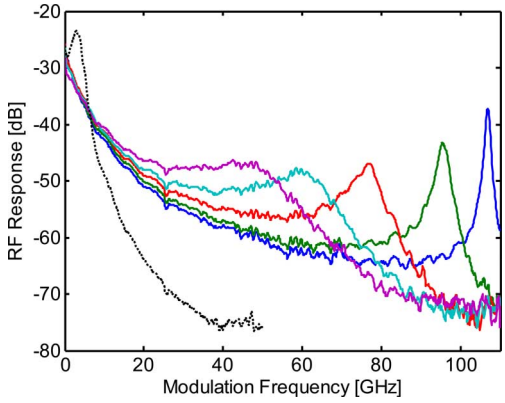

Fig. 6. Frequency response of an injection-locked DFB laser, showing $f_R = 45, 51, 61, 76, 96, 107$ GHz. $R = +14$ dB. $\Delta f = -22$, 3.5, 29, 54, 67 GHz. Dotted curve is the free-running response. The slave is biased at $1.3 \times J_{\rm th}$, which accounts for the low value of the first-order pole f_P.

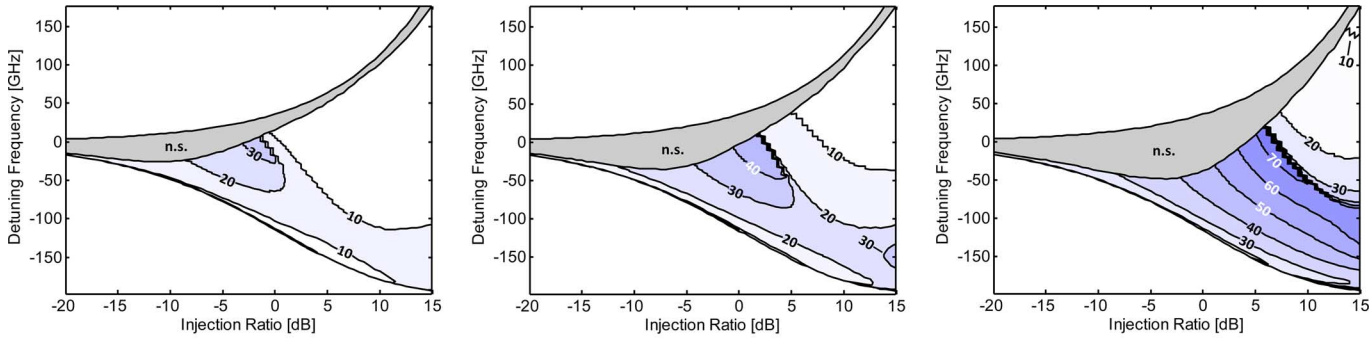

Fig. 7. Contour plot of 3-dB bandwidths (in GHz) across the locking range for (a) $J = 3 \times J_{\rm th}$, (b) $J = 5 \times J_{\rm th}$, and (c) $J = 10 \times J_{\rm th}$. The maximum 3-dB bandwidth increases with bias current. Note that (b) corresponds to the laser bias conditions in Fig. 3.

Fig. 8(a) shows experimental VCSEL frequency response curves (dotted) for 1.3 $\times$ and $5 \times J_{\rm th}$, plotted after de-embedding the RC parasitic pole, which we found to be 16 GHz. The slave laser's bias current was changed while maintaining a constant injection ratio ($\sim$12–13 dB) and resonance frequency (68 GHz). The RC pole was determined to be consistent by a fit over a wide range of resonance frequencies. The free-running output powers were -11 and -0.86 dBm, respectively. We observed an increase in the intrinsic 3-dB frequency from 1.5 to 80 GHz. Theoretical curves (solid), based on a small-signal analysis of the rate equations [55], match well to the experimental curves. An additional theoretical frequency response curve at $9 \times J_{\rm th}$ is given, showing the clear trend of bandwidth enhancement with increasing slave laser bias current. With a bias of $\geq 5 \times J_{\rm th}$, the 3-dB bandwidth extends beyond the resonance frequency, and we can achieve an intrinsic 3-dB bandwidth of 80 GHz. The extracted experimental pole frequencies are shown in Fig. 8(b). The figure shows that a pole enhancement of only $\sim$22 GHz (by biasing to $5 \times J_{\rm th}$) is needed to achieve the 80-GHz 3-dB bandwidth.

Of course, in practice, the laser modulation would ultimately be limited by RC parasitics rather than the intrinsic bandwidths. Note, however, that with the added benefit of being able to customize the damping factor, the RC parasitics can be compensated by decreasing the damping factor, thus using a slightly raised resonance peak to compensate for the RC low-pass filter response drop as an equalization technique.

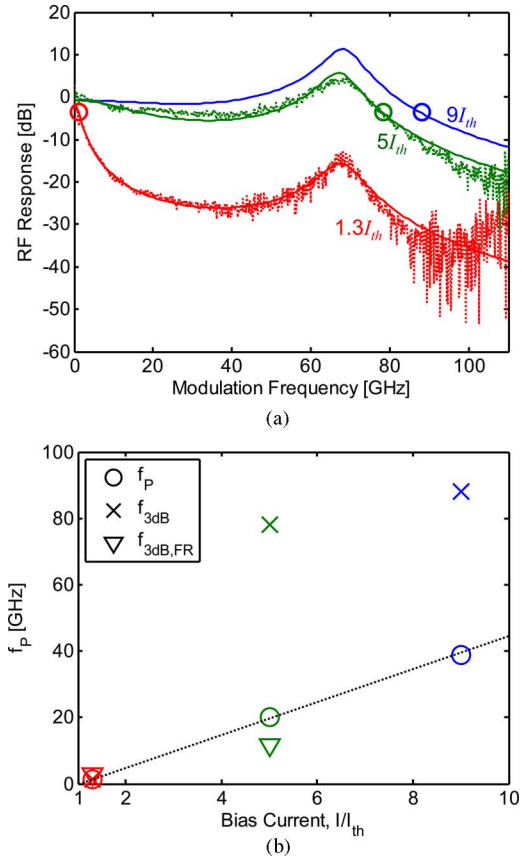

Fig. 8. (a) Experimental (dotted) and theoretical (solid) frequency responses of optical injection-locked VCSEL at different dc bias currents. 3-dB frequencies of 1.4 and 80 GHz for the experimental curves, respectively, are shown in circles. (b) Extracted first-order pole frequencies (f_P), with corresponding 3-dB frequencies ($f_{3\,\rm dB}$). Experimental free-running 3-dB frequencies ($f_{3\,\rm dB,FR}$) also marked.

D. Low-Frequency Gain

Strong injection locking has been experimentally shown to provide low-frequency direct-modulation response well above that of the free-running slave [20]. This gain can provide increased link performance at moderate bandwidths by combining the high optical power of the master laser (which may have poor modulation properties) with the optimized modulation properties of a directly modulated slave laser. As shown in Fig. 5, the RF gain typically occurs toward the negative detuning frequency edge of the locking range, where the resonance frequency is very low. Intuitively, when the laser is near the negative detuning edge, the extremely low-resonance frequency contributes to increase the dc gain. Here, we derive an analytical approximation for the dc gain.

At dc, the direct modulation response in (16) reduces to:

$$H(0) = \frac{gzS_0\left(\cos\phi_0 - \alpha\sin\phi_0\right)}{z^2\left(\gamma_N + gS_0\right) + gzS_0\left(\gamma_P - 2z\cos\phi_0\right)\left(\cos\phi_0 - \alpha\sin\phi_0\right)}. \quad (28)$$

The peak dc response is known to occur near the negative detuning frequency edge. Hence, for high injection ratios and a slave that is biased relatively well-above threshold, the photon number will be sufficiently larger such that we can approximate $\gamma_N \ll gS_0$. This reduces the response to:

$$H(0) = \frac{1}{z}\frac{1}{(\gamma_P/z) + [1/(\cos\phi_0 - \alpha\sin\phi_0)] - 2\cos\phi_0}. \tag{29}$$

If we wish to find the maximum dc response for a given injection power, we maximize (29) across the detuning range (in this case, ϕ_0). Although z is a function of ϕ_0, the dominant change occurs with the ϕ_0 terms, so z is treated as quasi-static, then solved later. This amounts to minimizing the two denominator terms that contain ϕ_0. Although complicated to minimize analytically, it turns out that for any value of $\alpha > 0$, the optimal ϕ_0 is well-approximated by $\phi_{\rm opt} \approx -0.1\pi$. By using the approximate value, the actual minimized function is matched with an error of $<1\%$ for any $\alpha > 1$.

To approximate S_0, in the strong injection regime ($R_{\rm inj} > 0$ dB) we solve the steady-state photon number in (8). This involves solving the cubic equation

$$0 = A_0^3 - BA_0^2 - A_{\rm fr}^2 A_0 - \frac{\gamma_N}{g}B, \tag{30}$$

where $B \equiv 2\kappa\tau_P A_{\rm inj}\cos\phi_{\rm opt}$; $\tau_P = 1/\gamma_P = Q_{\rm cav}/\omega_0$ is the photon lifetime. Using (13) and since $Q_c > Q_{\rm cav}$, $B \approx A_{\rm inj}Q_{\rm cav}/Q_c < A_{\rm inj}$. If the bias current is sufficiently above threshold, the final term in (30) can be neglected, giving

$$A_0 \approx \frac{B}{2} + \sqrt{\frac{B^2}{4} + S_{\rm fr}} = \frac{\delta A_{\rm inj}}{2}\left(1 + \sqrt{1 + \left(\frac{2A_{\rm fr}}{\delta A_{\rm inj}}\right)^2}\right) \tag{31}$$

where $\delta \equiv Q_{\rm cav}/Q_c$ and the injection ratio is taken to be sufficiently above 0 dB. Since $\cos\phi_{\rm opt} \approx 0.95$ and $B^2 > S_{\rm fr}$ and (31) approximates to

$$A_0 \approx \delta A_{\rm inj} + \frac{S_{\rm fr}}{\delta A_{\rm inj}}. \tag{32}$$

Hence, z approximates to

$$z \approx \frac{\gamma_P}{1.9}\frac{\rho}{\rho+1} \tag{33}$$

where $\rho \equiv R_{\rm inj}(0.95Q_{\rm cav}/Q_c)^2$. The maximum low-frequency response is thus approximately

$$H_{\rm DC,max} \approx H_{\rm DC,fr}\frac{\rho+1}{\rho/(1.8+0.59\alpha)+1} \tag{34}$$

where $H_{\rm dc,fr} = 1/\gamma_P$ is the low-frequency response of the free-running slave. Primarily, (34) can be used to argue that the maximum RF gain is mainly a factor of α and $R_{\rm inj}$. Hence, to optimize the dc response, one would want a large linewidth enhancement parameter α and injection ratio $R_{\rm inj}$. A large α is contrary to the design of a typical direct-modulated laser, although in this case it is desirable to obtain larger RF gain. Fig. 9 shows the numerical maximum low-frequency gain versus injection ratio, for different α values. Although increasing α also increases the low-frequency gain, there are diminishing returns.

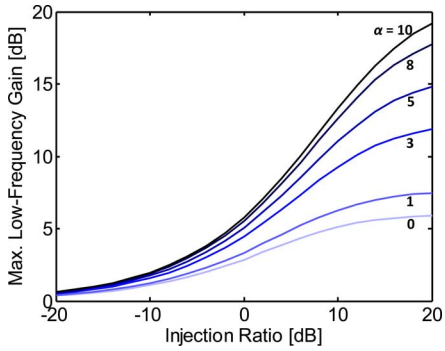

Fig. 9. Maximum low-frequency gain versus injection ratio, for various α.

One can see that the low-frequency gain can surpass the free-running laser's differential quantum efficiency.

As shown in Fig. 3(d), the high-gain, low-frequency response occurs away from the enhanced resonance frequency regime. Nevertheless, the maximum low-frequency gain can have significant bandwidth, as shown in Fig. 5, which shows a bandwidth of >20 GHz at the maximum low-frequency gain point. Since $\phi_{\rm opt}$ is close to 0, by observing (9), the detuning frequency at maximum low-frequency response will be at a negative frequency detuning for $\alpha > 0.32$, a valid condition for most semiconductor lasers.

E. Chirp

Chirp has also been studied in injection-locked lasers by several other authors [68], [69]. Piazzolla *et al.* [68] present a comprehensive small-signal analysis on the subject but does not fully consider the implications of strong injection locking. Relatively strong injection locking was explored by Yabre [69], but the study was mostly numerical. Here, we attempt to present a comprehensive analytical study of chirp in strong injection conditions.

The figure-of-merit for chirp is the magnitude of frequency deviation for a given power deviation or chirp-to-power ratio (CPR).

$$\mathrm{CPR_{OIL}} = \left|\frac{\Delta\omega}{\Delta S}\right| = \left|j\omega\frac{\Delta\phi}{\Delta S}\right| = \frac{\alpha}{2S_0}\left|j\omega\frac{j\omega+\omega_{\rm ZC}}{j\omega+\omega_{\rm PC}}\right| \tag{35}$$

$$\omega_{\rm ZC} = m_{SS} - \frac{m_{\phi S}m_{SN}}{m_{\phi N}} = z\left(\cos\phi_0 + \frac{1}{\alpha}\sin\phi_0\right) + \omega_{\rm ZC0}, \tag{36}$$

and

$$\omega_{\rm PC} = m_{\phi\phi} - \frac{m_{S\phi}m_{\phi N}}{m_{SS}} = z\left(\cos\phi_0 - \alpha\sin\phi_0\right). \tag{37}$$

The last term in (36) is defined as

$$\omega_{\rm ZC0} \equiv \varepsilon S_0 g(N_0 - N_{\rm tr}) \tag{38}$$

and is derived by the addition of gain compression into the rate equations, where we modeled the net stimulated gain as

$$g \rightarrow \frac{g}{1+\varepsilon S_0} \tag{39}$$

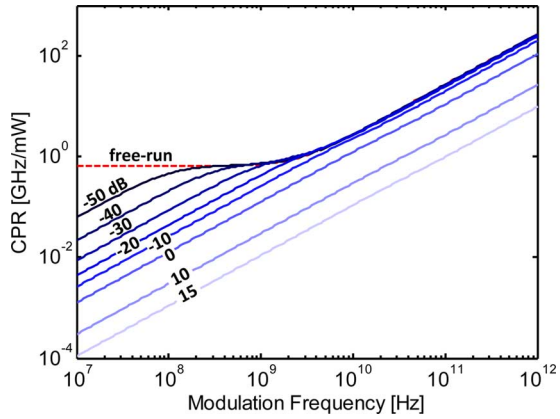

Fig. 10. CPR versus modulation frequency for various injection ratios, at a fixed phase of $\phi_0 = 0$.

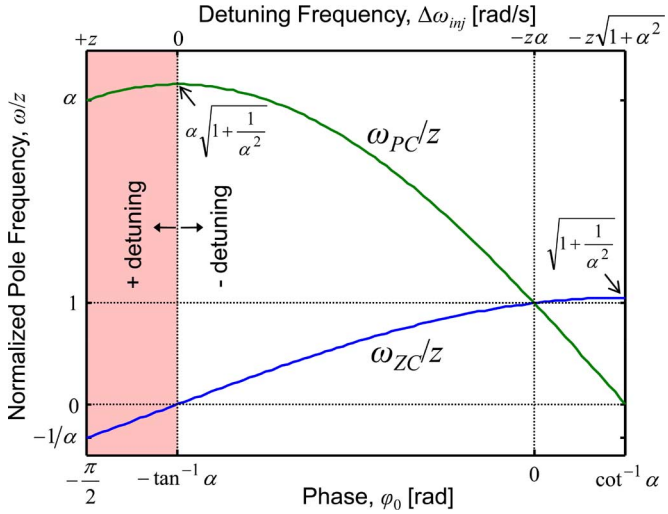

Fig. 11. Evolution of the CPR pole and zero frequency across the detuning range. The x-axis is linear with respect to phase with select detuning frequency values shown. Note that the zero is cancelled when $\Delta\omega_{\rm inj} = 0$ Hz.

and we assume $\varepsilon S_0 \ll 1$. Here, gain compression is needed to correctly model the dc chirp. While this dominates the dc chirp of a free-running laser, this term typically is in the range of 100 MHz and is only significant for low injection ratios.

The free-running laser can also be analyzed by the injection locking equations. For the free-running laser, there is no injected light. Therefore, $z = 0$, making $\omega_{\rm PC} = 0$. The free-running CPR becomes

$$\mathrm{CPR}_{\rm fr} = \frac{\alpha}{2S_0}\left|j\omega + \omega_{\rm ZC0}\right|. \tag{40}$$

This is consistent with the large-signal CPR model developed in [70] and the small-signal model in [67], [71]. Below $\omega_{\rm ZC0}$, the CPR is constant and proportional to $\alpha\varepsilon$. Slow changes in the photon number causes changes in the carrier number through gain compression. This, in turn, causes frequency shifts via the linewidth enhancement parameter.

Because of the existence of the nonzero pole, the dc chirp vanishes for injection-locked lasers. Essentially, the slave laser frequency attempts to stay locked to the master frequency. The frequency shifts due to α will be suppressed by changes in the phase difference between master and slave. As the modulation frequency increases, the attempted frequency deviations become larger and the restoring force cannot keep up, leading to a gradual increase in chirp.

When the injection ratio is decreased, the master power that is used to lock the slave becomes weaker, and the CPR becomes closer to the free-running case. This is shown in Fig. 10, where the phase is set to 0 and the injection ratio is varied. At $\phi_0 = 0$, at moderately high injection ratios, the pole and zero cancel each other, leaving a ω dependence on CPR. Note that the increased photon number for negative detunings allows the very high-frequency CPR to fall below the free-running value.

Fig. 11 shows the value of $\omega_{\rm PC}$ and $\omega_{\rm ZC}$ with respect to phase, assuming sufficiently strong injection ($z > \omega_{\rm ZC0}$). The CPR spectrum is also shown across the detuning range in Fig. 12. Note that the reduction of the zero frequency $\omega_{\rm ZC}$ by positive detuning also reduces the low-frequency CPR. By observing (35) for frequencies below $\omega_{\rm PC}$ (which corresponds to the useful modulation efficiency range), the CPR increases with α, as is the

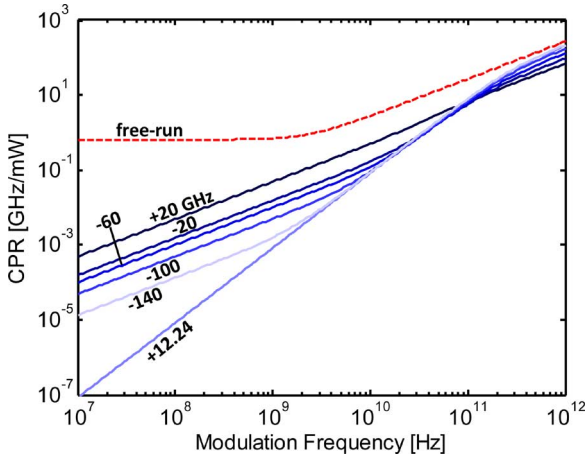

Fig. 12. CPR versus modulation frequency for various detuning frequencies across the locking range, at a fixed injection ratio $R_{\rm inj} = 4$ dB.

case with free-running laser. However, the CPR only increases for relatively small α and saturates for any value of $\alpha > 3$.

A special case is worth noting. When the detuning frequency is set to $\Delta\omega_{\rm inj} \approx 0$ (in actuality, slightly positive detuning), then $\omega_{\rm ZC} = 0$ and the injection-locked CPR is

$$\mathrm{CPR}_{\rm OIL}(\Delta\omega_{\rm inj} = 0) \approx \frac{\alpha}{2S_0}\left|\frac{\omega^2}{j\omega + z\sqrt{1+\alpha^2}}\right|. \tag{41}$$

This corresponds to the minimum low-frequency CPR for any given detuning. This is shown in Fig. 12, for $\Delta\omega_{\rm inj} = 12.24$ GHz. Detuning the master in either direction results in a nonzero $\omega_{\rm ZC}$ and an increase in the low-frequency chirp. The reasoning here is that the free-running dc chirp can be canceled by additional OIL dynamics.

F. Relative Intensity Noise

Intensity noise in free-running lasers is caused by random carrier recombination and generation events [72]. In OIL lasers,

the intensity and phase fluctuations of the injected light also contribute to the system's noise and cannot be ignored [12], [73]. OIL laser RIN has been studied using quantum mechanical approaches [74], [75] but only for reflection-style injection. Treatments using the phenomenological rate equations also exist in analytic [12], [73] and numerical [9]–[11] form, but do not include additional noise from reflected zero-point fluctuations at the laser facets that can significantly impact the output noise [76]. This difference between output and cavity noises can also be explained by partition noise derived from the output mirror reflectivity [72]. Here, we adopt an analytic approach that uses the phenomenological rate equations and takes the effect of zero-point fluctuations into account. Similar to the treatment in [12], we introduce Langevin noise sources to the rate equations, assuming that these sources are small enough that a small-signal treatment is valid.

Because spontaneous emission is negligible compared to other processes represented in the rate equations, we can ignore it in modulation response calculations without compromising accuracy. However, it is necessary to include the spontaneous emission rate in order to accurately model the Langevin noise spectral densities. We therefore introduce the terms $+R'_{\rm sp}$ in (1) and $-(R_{\rm sp}+R_{\rm nr})$ in (3), defining both as in [72]. We obtain the matrix equation as

$$\begin{bmatrix} m_{SS}+j\omega & m_{S\phi} & m_{SN} \\ m_{\phi S} & m_{\phi\phi}+j\omega & m_{\phi N} \\ m_{NS} & 0 & m_{NN}+j\omega \end{bmatrix} \begin{bmatrix} dS \\ d\phi \\ dN \end{bmatrix} = \begin{bmatrix} m_{Si} \\ m_{\phi i} \\ 0 \end{bmatrix} dS_{\rm inj} + \begin{bmatrix} m_{S\phi} \\ m_{\phi\phi} \\ 0 \end{bmatrix} d\phi_{\rm inj} + \begin{bmatrix} F_S \\ F_\phi \\ F_N \end{bmatrix} \quad (42)$$

where $m_{Si}=z\cos(\phi_0)S_0/S_{\rm inj}$ and $m_{\phi i}=-z\sin(\phi_0)/2$ $S_{\rm inj}dS$, $d\phi$, dN, $dS_{\rm inj}$, and $d\phi_{\rm inj}$ are the frequency-domain photon, phase, carrier, injected photon, and injected phase fluctuations, respectively. $dS_{\rm inj}$ and $d\phi_{\rm inj}$ contain the noise fluctuations added by the master laser. The RIN contributions from the master can be considered small-signal, broad-spectrum "modulation" of the injected master light. Hence, the master laser RIN contributions are very similar to the master modulation formulation found in [56]. F_S, F_ϕ, and F_N are the frequency-domain photon, phase, and carrier Langevin noise sources, respectively. Langevin noises are white (their spectral densities are independent of frequency), being stationary (so the Wiener–Khinchin theorem applies) and memoryless (so time-domain correlations are delta functions) processes [72]. Denoting the spectral density of the correlation between noises A and B as $\langle AB\rangle_\omega$ (where the subscript indicates any dependence on frequency), the photon noise spectral density from (42) and the Wiener–Khinchin theorem is

$$\begin{aligned}\langle dSdS\rangle_\omega = {} & |H_{SSi}(\omega)|^2\langle dS_{\rm inj}dS_{\rm inj}\rangle_\omega \\ & + |H_{S\phi i}(\omega)|^2\langle d\phi_{\rm inj}d\phi_{\rm inj}\rangle_\omega \\ & + |H_{SS}(\omega)|^2\langle F_SF_S\rangle + |H_{S\phi}(\omega)|^2\langle F_\phi F_\phi\rangle \\ & + |H_{SN}(\omega)|^2\langle F_NF_N\rangle \\ & + 2{\rm Re}\left\{H_{SSi}(\omega)\,H_{S\phi i}(\omega)^*\langle dS_{\rm inj}d\phi_{\rm inj}\rangle_\omega\right\} \\ & + 2{\rm Re}\left\{H_{SS}(\omega)\,H_{SN}(\omega)^*\langle F_SF_N\rangle\right\} \end{aligned} \quad (43)$$

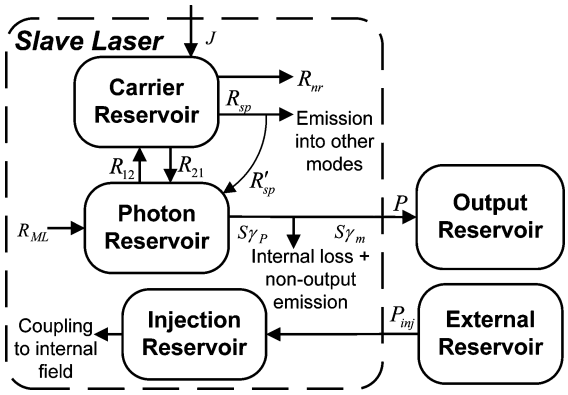

Fig. 13. Shot noise model diagram for the OIL laser system. Arrows are labeled by rate of particle flow within the laser and by power flow outside. $R_{\rm ML}$ is the rate of injection, defined as $R_{\rm ML}=2\kappa\sqrt{S_{\rm inj}S_0}\cos\phi_0$. R_{12} and R_{21} are the rates of stimulated emission and absorption, respectively. $P_{\rm inj}$ is the injected power and P is the slave laser output power.

where

$$\begin{aligned} H_{SS}(\omega) &= (m_{\phi\phi}+j\omega)(m_{NN}+j\omega)/D(\omega) \\ H_{S\phi}(\omega) &= -m_{S\phi}(m_{NN}+j\omega)/D(\omega) \\ H_{SN}(\omega) &= [m_{S\phi}m_{\phi N}-m_{SN}(m_{\phi\phi}+j\omega)]/D(\omega) \\ H_{SSi}(\omega) &= (m_{Si}(m_{\phi\phi}+j\omega)-m_{\phi i}m_{S\phi})(m_{NN}+j\omega)/D(\omega) \\ H_{S\phi i}(\omega) &= m_{S\phi}(m_{NN}+j\omega)\,j\omega/D(\omega) \end{aligned} \quad (44)$$

and $D(\omega)$ is the determinant of the coefficient matrix on the left side of (42). The output power spectral density is

$$\begin{aligned}\langle dPdP\rangle_\omega = {} & (h\nu\gamma_m)^2\langle dSdS\rangle_\omega + 2h\nu\gamma_m{\rm Re}\left\{H_{SS}(\omega)\langle F_SF_o\rangle\right\} \\ & + \langle F_oF_o\rangle, \end{aligned} \quad (45)$$

where F_o is the Langevin noise term associated with the output reservoir, γ_m is the rate of photon emission via the output facet, h is Planck's constant, and ν is the optical frequency of the slave laser output.

Fig. 13 gives the diagram for the shot noise model, first advanced by McCumber [77] and Lax [78], extended to the OIL laser context. In this model, the spectral density of a Langevin noise source's autocorrelation is simply the sum of all average rates of particle flow into and out of its reservoir. The spectral density of the cross-correlation between two noise sources is simply the negative of the sum of all average rates of particle flow between their reservoirs. Quantum noise due to zero-point fluctuations is accounted for via the external, injection, and output reservoirs and their associated noise sources.

We develop the theory for a slave laser with facets of equal power reflectivity r. Light is injected through one facet and the output power collected from the other facet. This model may be adapted to the case where power is injected through the output facet (via a circulator) but the contribution of reflected master laser light must then be taken into account [74]. The

slave laser is a DFB laser with typical parameters, obtained from [72]. Previous works have demonstrated the impact of injected noise on RIN [12], [73]. Here, we assume that the master laser operates at the quantum noise limit over the frequency range of interest. The intensity of the injected light is controlled by an attenuator between the master and the slave laser. Both master laser and attenuator are abstracted away by the external reservoir in Fig. 13. From Fig. 13 and the principles of the shot noise model, we calculate the spectral densities to be

$$\begin{aligned}
\langle F_S F_S \rangle &= 2R'_{\rm sp}(S_0+1) + 2R_{\rm ML} \\
\langle F_N F_N \rangle &= 2R'_{\rm sp}S_0 + 2R_{\rm nr} + 2R_{\rm sp} \\
\langle F_S F_N \rangle &= -(2R'_{\rm sp}S_0 - GS_0 + R'_{\rm sp}) \\
\langle F_o F_o \rangle &= h\nu P_0 \\
\langle F_S F_o \rangle &= -P_0 \\
\langle F_\phi F_\phi \rangle &= \langle F_S F_S \rangle / 4S_0^2 \\
\langle F_{\rm ext} F_{\rm ext} \rangle &= h\nu_{\rm ML} P_{\rm inj} \left[1 + (1-r)^{-1}\right] \\
\langle F_{\rm inj} F_{\rm inj} \rangle &= h\nu_{\rm ML} P_{\rm inj} \\
\langle F_{\rm ext} F_{\rm inj} \rangle &= -h\nu_{\rm ML} P_{\rm inj} \\
\langle dS_{\rm inj} dS_{\rm inj} \rangle_\omega &= (S_{\rm inj}/P_{\rm inj})^2 \cdot \{(1-r)^2 \langle F_{\rm ext} F_{\rm ext} \rangle \\
&\quad + 2(1-r)\langle F_{\rm ext} F_{\rm inj} \rangle + \langle F_{\rm inj} F_{\rm inj} \rangle\} \\
\langle d\phi_{\rm inj} d\phi_{\rm inj} \rangle_\omega &= (2-r) h\nu_{\rm ML} / 4P_{\rm inj}. \qquad (46)
\end{aligned}$$

All values in (46) are steady-state values. All other permutations of noise spectral densities that were not listed equate to 0. G is the total stimulated emission gain of the slave laser, where $G = g(N_0 - N_{\rm tr})$. P_0 denotes the steady-state slave laser output power. $F_{\rm ext}$ and $F_{\rm inj}$ are Langevin noise terms associated with the external and injection reservoirs, respectively. $+R'_{\rm sp}$, $R_{\rm nr}$, and $R_{\rm sp}$ are the rates of spontaneous emission into the mode, nonradiative recombination, and total spontaneous emission, respectively. $\nu_{\rm ML}$ is the optical frequency of the injected light. Since we are considering the case of stable injection locking, $\nu_{\rm ML} = \nu$. Combining equations (43)–(46), the single-sided noise spectrum relative intensity (RIN) may be obtained as

$$\mathrm{RIN}(\omega) = 2\langle dP dP \rangle_\omega / P_0^2. \qquad (47)$$

Fig. 14 shows the change in RIN as the external injection ratio is varied with a fixed detuning frequency of -5 GHz. In agreement with previous experiments [6], [20], [79], the OIL laser RIN characteristics in Fig. 14 depart from that of the slave laser and approach that of the quieter master laser as the injection ratio increases. In addition, the frequency of the RIN peak is increased by the stronger injection. As injection power is increased, the RIN at the peak decreases due to increased damping of the resonance. This was experimentally verified by Jin and Chuang [79]. Finally, we see that the conclusion in [12] that low-frequency OIL laser RIN is approximately invariant with injection strength holds only for the low levels of injection used in that study. Fig. 14 shows clearly that RIN at low frequencies can be suppressed significantly with high levels of injection.

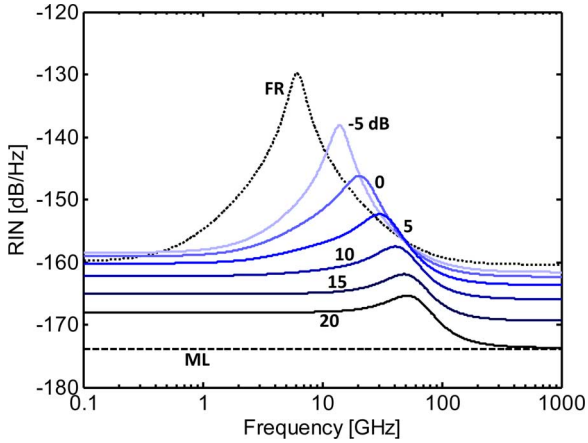

Fig. 14. RIN of OIL laser at a fixed detuning frequency of -5 GHz and various external injection ratios (as labeled). Dotted-line RIN plots of the free-running slave laser (FR SL) and master laser (ML) are included. The slave laser is biased at ten times its threshold current (4.5 mW).

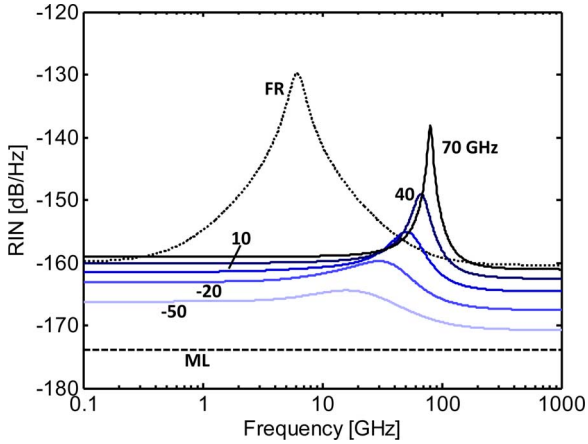

Fig. 15. Same conditions as Fig. 14 except the external injection ratio is fixed at 10 dB and detuning frequency varied (labeled).

Fig. 15 shows the behavior of RIN as the detuning frequency is varied for a fixed external injection ratio. As experimentally shown in [20], the RIN peak increases as one approaches the positive detuning edge (the phase difference between slave and injected light approaches $-\pi/2$). RIN generally decreases as detuning frequency decreases toward the point where the phase difference is 0 (maximum output power). That minimum RIN at a given injection level is achieved at maximum output power has been observed at low injection levels [73] and for the case where light is injected through the output facet [74]. We show here that this is also true for ultra-high optical injection into a nonoutput facet.

For high RF frequencies, the RIN approaches the quantum shot noise limit: $\mathrm{RIN} = 2h\nu/P_0$. For higher injection ratios and negative detuning, the shot noise is reduced, as shown in Figs. 14 and 15, due to the increasing output power from the slave cavity. It is interesting to note that it may be possible to reduce the quantum limit below both shot noise limits of the master and slave, since the output power of the slave, at negative detunings, can exceed the power of the solitary master

and slave (but not exceed the sum of master and slave power). This assumes, however, lossless coupling, in order to keep the locked power above both solitary master and slave lasers.

For low RF frequencies ($\omega \ll \omega R$), the slave laser's internal photon fluctuation is dominated by the dc response of the autocorrelation carrier noise term:

$$\langle dSdS \rangle_\omega \approx |H_{SN}(\omega)|^2 \langle F_N F_N \rangle \tag{48}$$

which results in an approximate low-frequency RIN of

$$\mathrm{RIN}(\omega = 0) = \frac{2h\nu}{P_0}\left[2\gamma_m R'_{\mathrm{sp}} |H_{SN}(\omega = 0)|^2 + 1\right]. \tag{49}$$

The second term implies that the RIN, as usual, cannot go below the standard quantum limit (unless squeezed). Interestingly, the term H_{SN} is the small-signal response in (16), evaluated at dc. This is proportional to the low-frequency RF gain as discussed in Section IV-D.

Note that while high injection and low detuning appear to favor low RIN, both these conditions also favor high output power levels, which may be unfeasible for transmission over optical fiber due to effects like stimulated Brouillon scattering. Although we investigate only intensity noise here, our model lends itself just as effectively to a study of frequency noise in an OIL laser system.

A few general trends of RIN in OIL lasers are noted. In many ways, the RIN follows that of a free-running laser. For example, the RIN peak follows the peak of the relaxation oscillation, both in frequency and amplitude. This is evident by observing that almost all terms in (45), save the output partition noise, share the same denominator (read: poles) as the small-signal response for direct modulation of the OIL laser found in (16). Hence, an increase in the peak direct modulation amplitude by positive detuning, for example, leads to a corresponding increase in the RIN peak amplitude. It is important to reiterate that the RIN peak frequency and amplitude can be modified by both detuning and injection ratio. In OIL, the relaxation oscillation frequency can increase, thus pushing the RIN peak to higher frequencies. This has been shown to be useful in reducing noise for modulation frequencies near the free-running resonance [20].

V. Conclusion

The classic differential equations for injection-locked lasers are used to describe many of the enhanced laser characteristics that OIL provides. Resonance frequency, damping, 3-dB bandwidth, chirp, and RIN are shown to be improved, depending on the locking parameters. We discuss the physical interpretation of the enhancements over the free-running case. We also delineate specific design parameters and locking conditions that can be used to optimize the injection-locked laser for different applications.

Acknowledgment

The authors wish to thank Prof. Connie Chang-Hasnain and Dr. Xiaoxue Zhao of the University of California, Berkeley, Prof. Lukas Chrostowski of the University of British Columbia, Vancouver, and Prof. Rod Tucker of the University of Melbourne, Melbourne, for helpful discussions.

References

[1] K. Nakahara, T. Tsuchiya, T. Kitatani, K. Shinoda, T. Taniguchi, T. Kikawa, M. Aoki, and M. Mukaikubo, "40-Gb/s direct modulation with high extinction ratio operation of 1.3-μm InGaAlAs multiquantum well ridge waveguide distributed feedback lasers," *IEEE Photon. Technol. Lett*, vol. 19, no. 19, pp. 1436–1438, Oct. 2007.

[2] T. Anan, N. Suzuki, K. Yashiki, K. Fukatsu, H. Hatakeyama, T. Akagawa, K. Tokutome, and M. Tsuji, "High-speed 1.1-μm-range InGaAs VCSELs," in *Proc. Opt. Fiber Commun. Conf.*, San Deigo, CA, 2008, pp. 1–3.

[3] K. Iwashita and K. Nakagawa, "Suppression of mode partition noise by laser diode light injection," *IEEE J. Quantum Electron.*, vol. 18, no. 10, pp. 1669–1674, Oct. 1982.

[4] C. H. Henry, N. A. Olsson, and N. K. Dutta, "Locking range and stability of injection locked 1.54 μm InGaAsP semiconductor lasers," *IEEE J. Quantum Electron.*, vol. QE-21, no. 8, pp. 1152–1156, Aug. 1985.

[5] A. Murakami, K. Kawashima, and K. Atsuki, "Cavity resonance shift and bandwidth enhancement in semiconductor lasers with strong light injection," *IEEE J. Quantum Electron.*, vol. 39, no. 10, pp. 1196–1204, Oct. 2003.

[6] T. B. Simpson, J. M. Liu, and A. Gavrielides, "Bandwidth enhancement and broadband noise reduction in injection-locked semiconductor lasers," *IEEE Photon. Technol. Lett.*, vol. 7, no. 7, pp. 709–711, Jul. 1995.

[7] X. J. Meng, T. Chau, D. T. K. Tong, and M. C. Wu, "Suppression of second harmonic distortion in directly modulated distributed feedback lasers by external light injection," *Electron. Lett.*, vol. 34, no. 21, pp. 2040–2041, Oct. 1998.

[8] L. Chrostowski, C. H. Chang, and C. Chang-Hasnain, "Reduction of relative intensity noise and improvement of spur-free dynamic range of an injection locked VCSEL," in *Proc. 16th Annu. Meet. IEEE Lasers Electro-Opt. Soc.*, vol. 2, Tuscon, AZ, IEEE, 2003, pp. 706–707.

[9] N. Schunk and K. Petermann, "Noise analysis of injection-locked semiconductor injection lasers," *IEEE J. Quantum Electron.*, vol. QE-22, no. 5, pp. 642–650, May 1986.

[10] M. C. España-Boquera and A. Puerta-Notario, "Noise effects in injection locked laser simulation: Phase jumps and associated spectral components," *Electron. Lett.*, vol. 32, no. 9, pp. 818–819, 1996.

[11] J. M. Liu, H. F. Chen, X. J. Meng, and T. B. Simpson, "Modulation bandwidth, noise, and stability of a semiconductor laser subject to strong injection locking," *IEEE Photon. Technol. Lett.*, vol. 9, no. 10, pp. 1325–1327, Oct. 1997.

[12] G. Yabre, H. De Waardt, H. P. A. Van Den Boom, and G. D. Khoe, "Noise characteristics of single-mode semiconductor lasers under external light injection," *IEEE J. Quantum Electron.*, vol. 36, no. 3, pp. 385–393, Mar. 2000.

[13] C. Lin and F. Mengel, "Reduction of frequency chirping and dynamic linewidth in high-speed directly modulated semiconductor lasers by injection locking," *Electron. Lett.*, vol. 20, no. 25–26, pp. 1073–1075, 1984.

[14] H. Toba, Y. Kobayashi, K. Yanagimoto, H. Nagai, and M. Nakahara, "Injection-locking technique applied to a 170 km transmission experiment at 445.8 Mbit/s," *Electron. Lett.*, vol. 20, no. 9, pp. 370–371, 1984.

[15] N. A. Olsson, H. Temkin, R. A. Logan, L. F. Johnson, G. J. Dolan, J. P. Van Der Ziel, and J. C. Campbell, "Chirp-free transmission over 82.5 km of single mode fibers at 2 Gbit/s with injection locked DFB semiconductor lasers," *J. Lightw. Technol.*, vol. 3, no. 1, pp. 63–67, Jan. 1985.

[16] H.-K. Sung, T. Jung, D. Tishinin, K. Y. Liou, W. T. Tsang, and M. C. Wu, "Optical injection-locked gain-lever distributed Bragg reflector lasers with enhanced RF performance," in *Proc. IEEE Int. Top. Meet. Microw. Photon.*, Ogunquit, ME, 2004, pp. 225–228.

[17] H.-K. Sung, E. K. Lau, and M. C. Wu, "Near-single sideband modulation in strong optical injection locked semiconductor lasers," presented at the Opt. Fiber Commun. Conf., Anaheim, CA, 2006.

[18] A. Umbach, G. Unterborsch, R. P. Braun, and G. Grobkopf, "Stable optical source and high-speed photodetector used for remote fiber-optic 64-GHz μm wave generation," in *Opt. Fiber Commun. Conf.*, San Jose, CA, 1998, pp. 260–261.

[19] L. Goldberg, A. M. Yurek, H. F. Taylor, and J. F. Weller, "35 GHz microwave signal generation with an injection-locked laser diode," *Electron. Lett.*, vol. 21, no. 18, pp. 814–815, 1985.

[20] L. Chrostowski, X. Zhao, and C. J. Chang-Hasnain, "Microwave performance of optically injection-locked VCSELs," *IEEE Trans. Microw. Theory Tech.*, vol. 54, no. 2, pp. 788–796, Feb. 2006.

[21] A. Kuramoto and S. Yamashita, "All-optical regeneration using a side-mode injection-locked semiconductor laser," *IEEE J. Sel. Topics Quantum Electron.*, vol. 9, no. 5, pp. 1283–1287, Sep.–Oct. 2003.

[22] B. Li, M. I. Memon, G. Yuan, Z. Wang, S. Yu, G. Mezosi, and M. Sorel, "All-optical response of semiconductor ring laser bistable to duo optical injections," in *Proc. Conf. Lasers Electro-Opt.*, San Jose, CA, 2008, pp. 1–2.

[23] L. Chrostowski and W. Shi, "Monolithic injection-locked high-speed semiconductor ring lasers," *J. Lightw. Technol.*, vol. 26, no. 19, pp. 3355–3362, Oct. 2008.

[24] A. Pikovsky, M. Rosenblum, J. Kurths, and B. Chirikov, "Synchronization: A universal concept in nonlinear sciences," in *Cambridge Nonlinear Science Series*. Cambridge, U.K.: Cambridge Univ. Press, 2003.

[25] J. H. Vincent, "On some experiments in which two neighboring maintained oscillator circuits affect a resonanting circuit," *Proc. Roy. Soc.*, vol. 32, no. 2, pp. 84–91, 1919–1920.

[26] E. V. Appleton, "The automatic synchronization of triode oscillators," in *Proc. Camb. Soc.*, vol. 21, pp. 231–248, 1922–1923.

[27] R. Adler, "A study of locking phenomena in oscillators," in *Proc. IRE*, 1946, vol. 34, pp. 351–357.

[28] T. H. Maiman, "Stimulated optical radiation in ruby," *Nature*, vol. 187, no. 4736, pp. 493–494, 1960.

[29] H. L. Stover and W. H. Steier, "Locking of laser oscillators by light injection," *Appl. Phys. Lett.*, vol. 8, no. 4, pp. 91–93, 1966.

[30] C. J. Buczek and R. J. Freiberg, "Hybrid injection locking of higher power CO_2 lasers," *IEEE J. Quantum Electron.*, vol. 8, no. 7, pp. 641–650, Jul. 1972.

[31] S. Kobayashi and T. Kimura, "Coherence on injection phase-locked AlGaAs semiconductor laser," *Electron. Lett.*, vol. 16, no. 7, pp. 668–670, 1980.

[32] R. H. Pantell, "The laser oscillator with an external signal," *Proc. IEEE*, vol. 53, no. 5, pp. 474–477, May 1965.

[33] C. L. Tang and H. Statz, "Phase-locking of laser oscillators by injected signal," *J. Appl. Phys.*, vol. 38, no. 1, pp. 323–324, 1967.

[34] K. Otsuka and S. Tarucha, "Theoretical studies on injection locking and injection-induced modulation of laser diodes," *IEEE J. Quantum Electron.*, vol. 17, no. 8, pp. 1515–1521, Aug. 1981.

[35] R. Lang, "Injection locking properties of a semiconductor laser," *IEEE J. Quantum Electron.*, vol. 18, no. 6, pp. 976–983, Jun. 1982.

[36] Y. Yamamoto, "Receiver performance evaluation of various digital optical modulation-demodulation systems in the 0.5–10 μm wavelength region," *IEEE J. Quantum Electron*, vol. 16, no. 11, pp. 1251–1259, Nov. 1980.

[37] S. Kobayashi and T. Kimura, "Optical phase modulation in an injection locked AlGaAs semiconductor laser," *IEEE J. Quantum Electron.*, vol. 18, no. 10, pp. 1662–1669, Oct. 1982.

[38] S. Kobayashi and T. Kimura, "Optical FM signal amplification by injection locked and resonant type semiconductor laser amplifiers," *IEEE J. Quantum Electron.*, vol. 18, no. 4, pp. 575–581, Apr. 1982.

[39] S. Kasapi, S. Lathi, and Y. Yamamoto, "Sub-shot-noise frequency-modulation spectroscopy by use of amplitude-squeezed light from semiconductor lasers," *J. Opt. Soc. Amer. B*, vol. 17, no. 2, pp. 275–279, 2000.

[40] A. A. Salles and J. R. Forrest, "Initial observations of optical injection locking of GaAs metal semiconductor field effect transistor oscillators," *Appl. Phys. Lett.*, vol. 38, no. 5, pp. 392–394, 1981.

[41] A. Seeds, J. Singleton, S. Brunt, and J. Forrest, "The optical control of IMPATT oscillators," *J. Lightw. Technol.*, vol. 5, no. 3, pp. 403–411, Mar. 1987.

[42] R. D. Esman, L. Goldberg, and J. F. Weller, "Optical phase control of an optically injection-locked FET microwave oscillator," *IEEE Trans. Microw. Theory Tech.*, vol. 37, no. 10, pp. 1512–1518, Oct. 1989.

[43] A. J. Seeds, I. D. Blanchflower, N. J. Gomes, G. King, and S. J. Flynn, "New developments in optical control techniques for phased array radar," in *Proc. IEEE MTT Int. Microw. Symp. Dig.*, 1988, pp. 905–908.

[44] L. Goldberg, H. F. Taylor, and J. F. Weller, "FM sideband injection locking of diode lasers," *Electron. Lett.*, vol. 18, no. 23, pp. 1019–1020, 1982.

[45] C. Lin, J. K. Andersen, and F. Mengel, "Frequency chirp reduction in a 2.2 Gbit/s directly modulated InGaAsP semiconductor laser by CW injection," *Electron. Lett.*, vol. 21, no. 2, pp. 80–81, 1985.

[46] S. Saito, F. Mogensen, and H. Olesen, "Effective bandwidth for FM noise suppression in an injection-locked semiconductor laser," *Electron. Lett.*, vol. 21, no. 24, pp. 1173–1175, 1985.

[47] F. Mogensen, H. Olesen, and G. Jacobsen, "FM noise suppression and linewidth reduction in an injection-locked semiconductor laser," *Electron. Lett.*, vol. 21, no. 16, pp. 696–697, 1985.

[48] F. Mogensen, H. Olesen, and G. Jacobsen, "Locking conditions and stability properties for a semiconductor laser with external light injection," *IEEE J. Quantum Electron.*, vol. QE-21, no. 7, pp. 784–793, Jul. 1985.

[49] X. J. Meng, T. Jung, T. Chau, and M. C. Wu, "Gain and bandwidth enhancement of directly modulated analog fiber optic links using injection-locked gain-coupled DFB lasers," in *Proc. IEEE Int. Top. Meet. Microw. Photon.*, Melbourne, VIC, Australia, 1999, pp. 141–144.

[50] X. J. Meng, T. Chau, and M. C. Wu, "Improved intrinsic dynamic distortions in directly modulated semiconductor lasers by optical injection locking," *IEEE Trans. Microw. Theory Tech.*, vol. 47, no. 7, pp. 1172–1176, Jul. 1999.

[51] E. K. Lau, X. Zhao, H.-K. Sung, D. Parekh, C. Chang-Hasnain, and M. C. Wu, "Strong optical injection-locked semiconductor lasers demonstrating $>$ 100-GHz resonance frequencies and 80-GHz intrinsic bandwidths," *Opt. Exp.*, vol. 16, no. 9, pp. 6609–6618, 2008.

[52] E. K. Lau, H.-K. Sung, and M. C. Wu, "Ultra-high, 72 GHz resonance frequency and 44 GHz bandwidth of injection-locked 1.55-μm DFB lasers," in *Proc. Opt. Fiber Commun. Conf.*, Anaheim, CA, 2006, pp. 1–3.

[53] L. Chrostowski, B. Faraji, W. Hofmann, R. Shau, M. Ortsiefer, and M. C. Amann, "40 GHz bandwidth and 64 GHz resonance frequency in injection-locked 1.55 μm VCSELs," in *Proc. Int. Semicond. Laser Conf.*, Kohala Coast, HI, 2006, pp. 117–118.

[54] L. Chrostowski, B. Faraji, W. Hofmann, M. C. Amann, S. Wieczorek, and W. W. Chow, "40 GHz bandwidth and 64 GHz resonance frequency in injection-locked 1.55 μm VCSELs," *IEEE J. Sel. Topics Quantum Electron.*, vol. 13, no. 5, pp. 1200–1208, Sep.–Oct. 2007.

[55] E. K. Lau, H.-K. Sung, and M. C. Wu, "Frequency response enhancement of optical injection-locked lasers," *IEEE J. Quantum Electron.*, vol. 44, no. 1, pp. 90–99, Jan. 2008.

[56] E. K. Lau, L. J. Wong, X. Zhao, Y.-K. Chen, C. J. Chang-Hasnain, and M. C. Wu, "Bandwidth enhancement by master modulation of optical injection-locked lasers," *J. Lightw. Technol.*, vol. 26, no. 15, pp. 2584–2593, Aug. 2008.

[57] A. Markus, J. X. Chen, O. Gauthier-Lafaye, J. G. Provost, C. Paranthoen, and A. Fiore, "Impact of intraband relaxation on the performance of a quantum-dot laser," *IEEE J. Sel. Topics Quantum Electron.*, vol. 9, no. 5, pp. 1308–1314, Sep.–Oct. 2003.

[58] T. C. Newell, D. J. Bossert, A. Stintz, B. Fuchs, K. J. Malloy, and L. F. Lester, "Gain and linewidth enhancement factor in InAs quantum-dot laser diodes," *IEEE Photon. Technol. Lett.*, vol. 11, no. 12, pp. 1527–1529, Dec. 1999.

[59] Y. Wan, X. Lai, and J. Roychowdhury, "Understanding injection locking in negative-resistance *LC* oscillators intuitively using nonlinear feedback analysis," in *Proc. IEEE Custom Integr. Circuits Conf. (CICC)*, Sep. 2005, pp. 729–732.

[60] E. K. Lau, H.-K. Sung, and M. C. Wu, "Scaling of resonance frequency for strong injection-locked lasers," *Opt. Lett.*, vol. 32, no. 23, pp. 3373–3375, 2007.

[61] T. B. Simpson, S. Wieczorek, B. Krauskopf, and D. Lenstra, "Mapping the complex dynamics of a semiconductor laser subject to optical injection," in *Proc. AIP Conf.*, 2003, pp. 375–375.

[62] T. B. Simpson, J. M. Liu, A. Gavrielides, V. Kovanis, and P. M. Alsing, "Period-doubling route to chaos in a semiconductor laser subject to optical injection," *Appl. Phys. Lett.*, vol. 64, no. 26, pp. 3539–3541, 1994.

[63] V. Annovazzi-Lodi, S. Donati, and M. Manna, "Chaos and locking in a semiconductor laser due to external injection," *IEEE J. Quantum Electron.*, vol. 30, no. 7, pp. 1537–1541, Jul. 1994.

[64] X. J. Meng, T. Chau, and M. C. Wu, "Experimental demonstration of modulation bandwidth enhancement in distributed feedback lasers with external light injection," *Electron. Lett.*, vol. 34, no. 21, pp. 2031–2032, Oct. 1998.

[65] X. Zhao, D. Parekh, E. K. Lau, H.-K. Sung, M. C. Wu, and C. J. Chang-Hasnain, "Optoelectronic oscillator using injection-locked VCSELs," in *Proc. Annu. Meet. IEEE Lasers Electro-Opt. Soc.*, Lake Buena Vista, FL, 2007, pp. 190–191.

[66] H.-K. Sung, E. K. Lau, X. Zhao, D. Parekh, C. J. Chang-Hasnain, and M. C. Wu, "Optically injection-locked optoelectronic oscillators with low RF threshold gain," in *Proc. Conf. Lasers Electro-Opt.* Baltimore, MD, 2007, pp. 1–2.

[67] R. S. Tucker, "High-speed modulation of semiconductor lasers," *J. Lightw. Technol.*, vol. 3, no. 6, pp. 1180–1192, 1985.

[68] S. Piazzolla, P. Spano, and M. Tamburrini, "Small signal analysis of frequency chirping in injection-locked semiconductor lasers," *IEEE J. Quantum Electron.*, vol. QE-22, no. 12, pp. 2219–2223, Dec. 1986.
[69] G. Yabre, "Effect of relatively strong light injection on the chirp-to-power ratio and the 3 dB bandwidth of directly modulated semiconductor lasers," *J. Lightw. Technol.*, vol. 14, no. 10, pp. 2367–2373, Oct. 1996.
[70] T. L. Koch and R. A. Linke, "Effect of nonlinear gain reduction on semiconductor laser wavelength chirping," *Appl. Phys. Lett.*, vol. 48, no. 10, pp. 613–615, 1986.
[71] D. Welford, "A rate equation analysis for the frequency chirp to modulated power ratio of a semiconductor diode laser," *IEEE J. Quantum Electron.*, vol. 21, no. 11, pp. 1749–1751, Nov. 1985.
[72] L. A. Coldren and S. W. Corzine, *Diode Lasers and Photonic Integrated Circuits*. New York: Wiley, 1995.
[73] P. Spano, S. Piazzolla, and M. Tamburrini, "Frequency and intensity noise in injection-locked semiconductor lasers: Theory and experiments," *IEEE J. Quantum Electron.*, vol. 22, no. 3, pp. 427–435, Mar. 1986.
[74] L. Gillner, G. Björk, and Y. Yamamoto, "Quantum noise properties of an injection-locked laser oscillator with pump-noise suppression and squeezed injection," *Phys. Rev. A*, vol. 41, no. 9, pp. 5053–5065, 1990.
[75] H. A. Haus and Y. Yamamoto, "Quantum noise of an injection-locked laser oscillator," *Phys. Rev. A*, vol. 29, no. 3, pp. 1261–1274, 1984.
[76] Y. Yamamoto and N. Imoto, "Internal and external field fluctuations of a laser oscillator: Part I-Quantum mechanical Langevin treatment," *IEEE J. Quantum Electron.*, vol. 22, no. 10, pp. 2032–2042, Oct. 1986.
[77] D. E. McCumber, "Intensity fluctuations in the output of CW laser oscillators. I," *Phys. Rev.*, vol. 141, no. 1, pp. 306–322, 1966.
[78] M. Lax, "Classical noise IV: Langevin methods," *Rev. Mod. Phys.*, vol. 38, no. 3, pp. 541–566, 1966.
[79] X. Jin and S. L. Chuang, "Relative intensity noise characteristics of injection-locked semiconductor lasers," *Appl. Phys. Lett.*, vol. 77, no. 9, pp. 1250–1252, 2000.

Erwin K. Lau (S'01–M'06) received the B.S. and M.Eng. degrees in electrical engineering from Massachusetts Institute of Technology, Cambridge, in 2000 and 2001, respectively, and the Ph.D. degree in electrical engineering and computer sciences from the University of California, Berkeley, in 2006.

In 2004, he spent a summer at the IBM Thomas J. Watson Research Center, Yorktown, NY, where he worked on noise of parallel digital optical interconnects. He is currently a Postdoctoral Researcher in electrical engineering at the University of California, Berkeley. His research interests include optical injection locking of semiconductor lasers, nanocavity light emitters, and high-speed optical communications.

Dr. Lau is a member of the Optical Society of America. He was a 2002–2003 Hertz Fellowship Finalist.

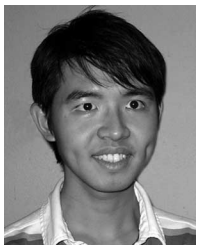

Liang Jie Wong received the B.S. degree in electrical engineering and computer science from the University of California, Berkeley, in 2008.

Since August 2008, he has been a Research Officer in the RF and Optical Department, Institute for Infocomm Research, Singapore. He is a National Science Scholar of the Agency for Science, Technology and Research (A∗STAR), Singapore. His current research interests include optical communications, quantum electronics, and laser noise theory.

Ming C. Wu (S'82–M'83–SM'00–F'02) received the M.S. and Ph.D. degrees in electrical engineering from the University of California, Berkeley, in 1985 and 1988, respectively.

From 1988 to 1992, he was a Member of the Technical Staff at AT& T Bell Laboratories, Murray Hill, NJ. From 1992 to 2004, he was a Professor in the Electrical Engineering Department, University of California, Los Angeles. He is currently a Professor of electrical engineering and computer sciences at the University of California, Berkeley, where he is also a Co-Director of Berkeley Sensor and Actuator Center (BSAC). His research interests include microelectromechanical systems and nanoelectromechanical systems, optofluidics, optoelectronics, nanophotonics, and biophotonics. He has authored or coauthored six book chapters, 140 journals, and 300 conference papers and holds 16 U.S. patents.

Prof. Wu is a member of the Optical Society of America. He was a Packard Foundation Fellow from 1992 to 1997 and received the 2007 Engineering Excellence Award from the Optical Society of America.